JOURNAL OF GEOPHYSICAL RESEARCH
MAY 2001; 106(B5) : 8521-8543
http://dx.doi.org/10.1029/2000JB900394

An edited version of this paper was published by AGU.

Variations in axial morphology, segmentation, and seafloor roughness along the Pacific-Antarctic Ridge between 56°S and 66°S

Hélène Ondréas[1], Daniel Aslanian[1], Louis Géli[1], Jean-Louis Olivet[1] and Anne Briais[2]

[1]Département des Géosciences Marines, Institut Français de Recherche et d'Exploitation de la Mer Plouzané, France
[2]Laboratoire d'Etudes en Géophysique et Océanographie Spatiale, Observatoire Midi-Pyrénées, CNRS Toulouse, France

Abstract:

The spreading rate at the Pacific-Antarctic Ridge (PAR) increases rapidly from 54 mm/yr near Pitman Fracture Zone (FZ) up to 76 mm/yr near Udintsev FZ, resulting in three domains of axial morphology: an axial valley south of Pitman FZ, an axial high north of Saint Exupéry FZ, and in between, the transitional domain extends over 650 km. It comprises sections of ridge with an axial valley or an axial high and generally displays a very low cross-sectional relief. It is also characterized by two propagating rifts. Two domains of different seafloor roughness appear south of Udintsev FZ: east of 157 °W these two domains are separated by a 1000-km V-shaped boundary. West of 157 °W, the boundary approximately coincides with Chron 3a or Chron 4. The southward migration of the transitional area during the last 35 Myr explains the V-shaped boundary: (1) increases in spreading rate above a threshold value produced changes in axial morphology; and (2) in the transition zone, rotations of the spreading direction were accommodated by the plate boundary, either by rift propagation or by transitions from fracture zones to non transform discontinuities, leaving trails on the seafloor that presently delineate the V. Seafloor roughness variations are not controlled by exactly the same spreading rate dependence as changes in axial morphology. The transition from rough to smooth seems to have occurred everywhere for spreading rates greater than 50 mm/yr, except in a domain presently centered on Saint-Exupéry FZ, where it occurred for spreading rates >60 to 65 mm/yr. Independent results from melting model calculations of major elements [*Vlastelic*et al., 2000] indicate that the upper mantle temperature is likely to be cooler between Antipodes and La Rose FZs. The combination of these two results reveals the existence of a 700-km-long segmentation of the upper mantle, with a "cool" area centered on Saint-Exupéry FZ.

JOURNAL OF GEOPHYSICAL RESEARCH, VOL. 106, NO B5, PAGES 8,521-8,543, MAY 10, 2001

Variations in axial morphology, segmentation, and seafloor roughness along the Pacific-Antarctic Ridge between 56°S and 66°S

Hélène Ondréas[1], Daniel Aslanian[1], Louis Géli[1], Jean-Louis Olivet[1] and Anne Briais[2]

[1]Département des Géosciences Marines, Institut Français de Recherche et d'Exploitation de la Mer Plouzané, France

[2]Laboratoire d'Etudes en Géophysique et Océanographie Spatiale, Observatoire Midi-Pyrénées, CNRS Toulouse, France

Abstract. The spreading rate at the Pacific-Antarctic Ridge (PAR) increases rapidly from 54 mm/yr near Pitman Fracture Zone (FZ) up to 76 mm/yr near Udintsev FZ, resulting in three domains of axial morphology: an axial valley south of Pitman FZ, an axial high north of Saint Exupéry FZ, and in between, the transitional domain extends over 650 km. It comprises sections of ridge with an axial valley or an axial high and generally displays a very low cross-sectional relief. It is also characterized by two propagating rifts. Two domains of different seafloor roughness appear south of Udintsev FZ: east of 157°W these two domains are separated by a 1000-km V-shaped boundary. West of 157°W, the boundary approximately coincides with Chron 3a or Chron 4. The southward migration of the transitional area during the last 35 Myr explains the V-shaped boundary: (1) increases in spreading rate above a threshold value produced changes in axial morphology; and (2) in the transition zone, rotations of the spreading direction were accommodated by the plate boundary, either by rift propagation or by transitions from fracture zones to non transform discontinuities, leaving trails on the seafloor that presently delineate the V. Seafloor roughness variations are not controlled by exactly the same spreading rate dependence as changes in axial morphology. The transition from rough to smooth seems to have occurred everywhere for spreading rates greater than 50 mm/yr, except in a domain presently centered on Saint-Exupéry FZ, where it occurred for spreading rates >60 to 65 mm/yr. Independent results from melting model calculations of major elements [*Vlastelic et al.*, 2000] indicate that the upper mantle temperature is likely to be cooler between Antipodes and La Rose FZs. The combination of these two results reveals the existence of a 700-km-long segmentation of the upper mantle, with a "cool" area centered on Saint-Exupéry FZ.

1. Introduction

Over the last 35 years the scientific community has focused much interest on the comparative study of "slow" and "fast" spreading ridges, mainly the slow Mid-Atlantic Ridge and the fast East Pacific Rise. Because of their remoteness from the North American and European oceanographic bases, the "intermediate" spreading centers of the southern oceans have been surveyed using modern multibeam techniques only in the last few years, in spite of their potential for understanding the transition between the two styles of accretion. A recent geophysical and geochemical survey of the South east Indian Ridge (SEIR) has shown that while the spreading rate remains nearly constant (70 to 75 mm/yr) between 88°E and 118°E, other parameters (such as variations in the upper mantle temperature and melt production) play an important role in shaping the axial relief and controlling the accretion processes [*Cochran et al.*, 1997; *Sempéré et al.*, 1997]. Here, we report data from the Pacific-Antarctic Ridge (PAR) between 65°30'S and Udintsev Fracture Zone (FZ), which exhibits exactly the opposite characteristics compared to the SEIR between 88°E and 118°E. (1) In contrast to what is observed along the SEIR, the PAR is devoid of any hot/cold spot influence, so that changes in mantle temperature or mantle heterogeneites underneath the spreading axis cannot be readily
ascribed to the presence of a nearby large-scale mantle temperature anomaly [*Géli et al.*, 1997; *Vlastelic et al.*, 2000]. (2) Owing to the proximity of the Euler pole of rotation between the Antarctic and the Pacific Plates, the spreading rate increases along the PAR from 54 mm/yr near 65°30'S up to 76 mm/yr near Udintsev FZ, spanning a wide range of spreading rates, from slow to fast.

In previous publications, we have presented general results [*Géli et al.*, 1997] and a study of the chemical systematics [*Vlastelic et al.*, 2000] of the Pacific-Antarctic Ridge south of the Udintsev FZ. Here we present a detailed, geological study of the present-day, ridge axial morphology and segmentation and their variations in time, aiming at (1) describing the along-axis variations of the geometry, segmentation, and morphology of the Pacific/Antarctic plate boundary; (2) correlating variations in axial relief with other observables; (3) assessing the role of changes in the Pacific and Antarctic Plates relative motion for shaping the geometry and the axial morphology of the plate boundary ; and (4) interpreting the changes in seafloor roughness that appear on the high resolution satellite gravity map of the Pacific-Antarctic area.

2. Geological Setting

2.1. Tectonic History

On the basis of detailed magnetic and multibeam data acquired in a 60-km-wide corridor along the Pitman FZ (Figure 1a), *Cande et al.* [1995] have reconstructed the relative motion of the Pacific and Antarctic Plates during the Cenozoic. The present-day Euler pole of rotation of the Pacific Plate relative to the Antarctic Plate is located near 67°S, 96°E, and the angular rotation rate is 2.42°/Myr, resulting in a regular, along-axis increase in spreading rate from 54 to 76 mm/yr

between 66°S and 56°S. The Pacific-Antarctic relative plate motion is characterized by a counter clockwise rotation of the spreading direction from Chron 27 (circa 61 Ma) to about Chron 6c (circa 24 Ma) and a clockwise rotation since about Chron 5a (12 Ma). Owing to the specific location of the Euler pole during the Cenozoic (in the area of the Wilkes and George V Lands, in Antarctica) the changes in spreading directions recorded in the geometry of the plate boundary are much larger on the south western end of the ridge, explaining the sharp bends in the south western fracture zones. In recent times, a sudden, major change occurred near the young end of Chron 3a (5.9 Ma) clearly recorded by a sharp rotation of about ~ 8° of the abyssal hill fabric near the Pitman FZ [*Macario et al.*, 1994], and two minor changes occurred at Chron 2a (circa 2.58 Ma) and Chron 1 (circa 0.78 Ma) respectively. The evolution of the Pacific/Antarctic plate boundary west of 180°W into a series of short, en échelon spreading segments appears to result from the changes in the relative plate motion during the late Neogene [*Cande et al.*, 1995]. We will show that these changes are also responsible for rearrangements in the geometry and segmentation of the Pacific-Antarctic spreading center between 180°W and Udintsev FZ.

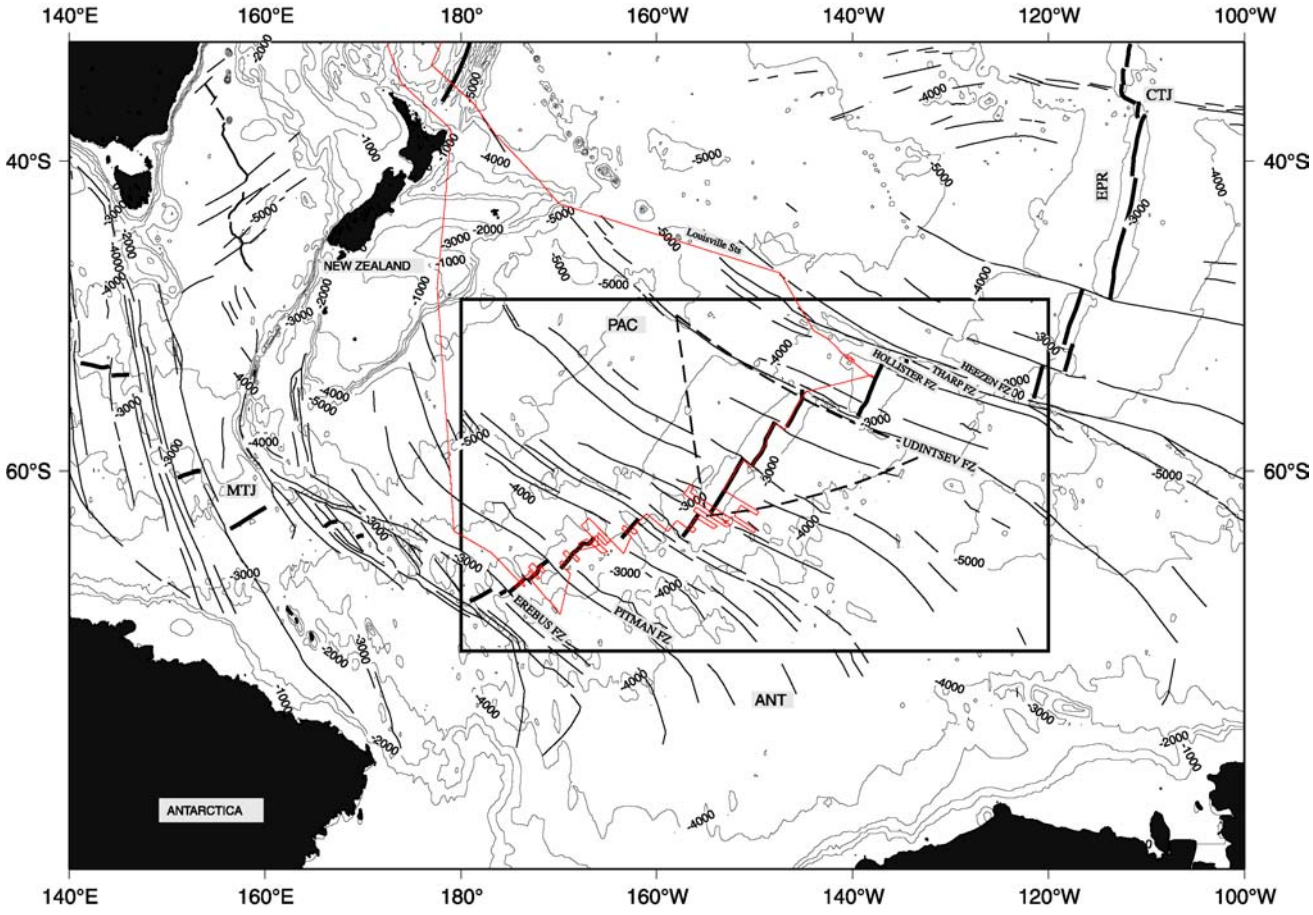

Figure 1a. Regional map of the Pacific-Antarctic basins indicating survey area (inset). Black lines indicate track-lines of R/V L'Atalante during Pacantarctic cruise, in 1996. CTJ, Chile Triple Junction; MTJ, Macquarie Triple Junction; EPR, East Pacific Rise; PAC, Pacific Plate; ANT, Antarctic Plate. Solid black line indicates accreting plate boundaries; thin black line is for fracture zones.

2.2. Satellite Altimetry Observations of a Large V-Shaped Boundary

Two domains of different satellite gravity signature [*Smith and Sandwell*, 1995] appear along the axis and on the adjacent basins of the Pacific-Antarctic Ridge between Udintsev FZ and 180°W: one of rough seafloor, with a high density of apparent, well marked fracture zones, and one of smooth seafloor comparable with the oceanic basins that have generally been formed at fast spreading centers. East of 157°W, these two domains are separated by a large V-shaped boundary, extending for more than 1000 km along the rise axis. According to *Sahabi et al.* [1996] this large-scale feature, which initiated shortly before Chron 13o, reflects a change in axial morphology that progressively propagated southwards since 35 Ma: as the Euler pole of rotation was moving to the southwest (away from the PAR) and as the spreading rate was becoming greater than a threshold value, the ridge axial morphology systematically changed from a valley to a high. *Géli et al.* [1997] further proposed that the large "V" may also reflect changes in axial segmentation and geometry (in addition to changes in axial morphology) that propagated southward since Oligocene times. In the present paper, we study the transition in seafloor roughness over the entire area, east and west of 157°W, and show that changes in seafloor roughness are not controlled by exactly the same spreading rate dependence as changes in axial morphology.

3. Axial Morphology and Geometry of the Present-Day Plate Boundary

Between January 6 and February 20 1996, the PACANTARCTIC cruise of R/V *L'Atalante* aimed at the geochemical and geophysical study of the Pacific-Antarctic Ridge, north of 65°35'S, 170°W and south of the Udintsev FZ (Figures 1a and 1b). Together with swath bathymetry [*Bourillet et al.*, 1996] and imagery [*Augustin et al.*, 1994] collected with the multibeam echosounder system, R/V *L'Atalante* acquired magnetic data with both a proton magnetometer towed behind the ship and a shipboard three-component magnetometer. Twenty-six rock samples have also been collected along 960 nautical miles of ridge axis including five from the Hollister Ridge, an oblique, aseismic structure between the Udintsev FZ and the Eltanin fault system [*Vlastelic et al.*, 1998; *Géli et al.,* 1998].

Basically, the PAR south of Udintsev FZ is divided into three domains of different morphologies: the southern area (Z1), between 65°30' S, 174°40'W and 64°40'S, 172°W, displays an axial valley similar (although less pronounced) to that observed at slow to intermediate spreading centers; the northern area (Z3), northeast of 63°10'S, 157°20'W, has an axial dome characteristic of fast spreading centers. In between, the 650-km-long transition zone (Z2) shows sections of ridges with axial highs, rifted highs, and axial valleys (Figure 1b).

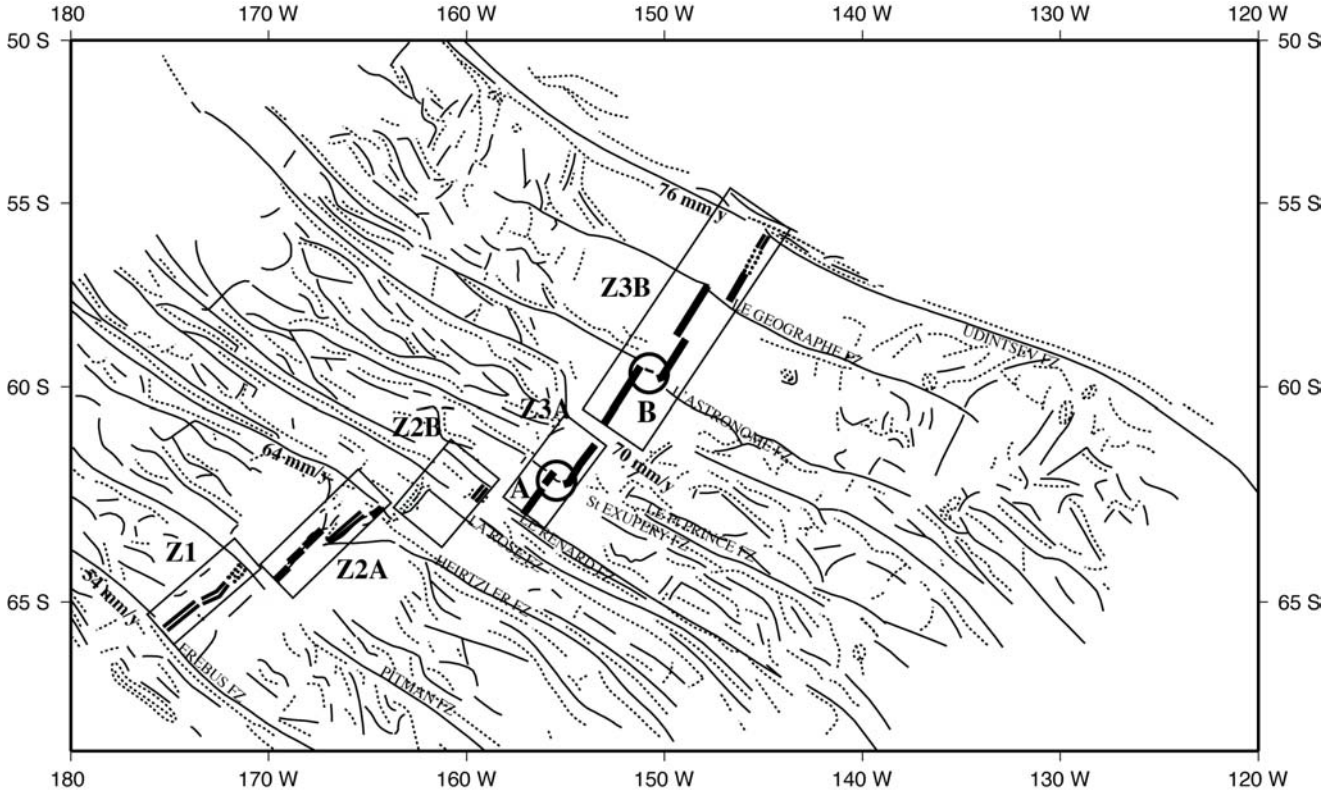

Figure 1b. Major structural features of studied area derived from 1-min grid satellite gravity map (D. Sandwell, personal communication, 2000). Black lines indicate gravity lows; dotted black lines indicate gravity highs. The spreading axis location is based on R/V *L'Atalante* data; it is marked by double black lines where a rift valley is present, in thick black line where a dome is present, and by dotted lines where the morphology is flat. Half spreading rate is indicated at places where the new data helped to determine it precisely. Axial morphology in insets Z1, Z2A, Z2B, Z3A, and Z3B is shown in Plates 1, 2, 3, 4, and 5 respectively

3.1. Zone 1: Slow Spreading Morphology

Zone 1 extends from 70 km northeast of the Erebus FZ (southern boundary of our survey) to the N140 Pitman FZ (Figure 1b and Plate 1) and shows axial valley morphology. Following the nomenclature of *Macdonald et al.* [1991], the axis is divided into three second-order segments named Z1-S1, Z1-S2, and Z1-S3. The segments are offset by two second-order discontinuities named Z1-D1 and Z1-D2 (Table 1). The clearly defined axial magnetic anomaly (Plate 1) is used to locate the position of the active spreading center and estimate a spreading rate of 54 to 56 mm/yr all over the area.

Two observations in zone 1 contrast with what is usually observed on mid-ocean ridges: (1) the change in axial morphology from deep rift valley to a platform along segment Z1-S3 is not related to any axial discontinuity and occurs over a distance of 40 km only (Figure 2 and Plate 1); (2) while the axial seafloor plunges by about 500 to 800 m near the extremities of segments Z1-S1 and Z2-S2 as generally observed along mid-ocean ridges [e.g., *Macdonald et al.*, 1992], it does not deepen approaching the Pitman FZ.

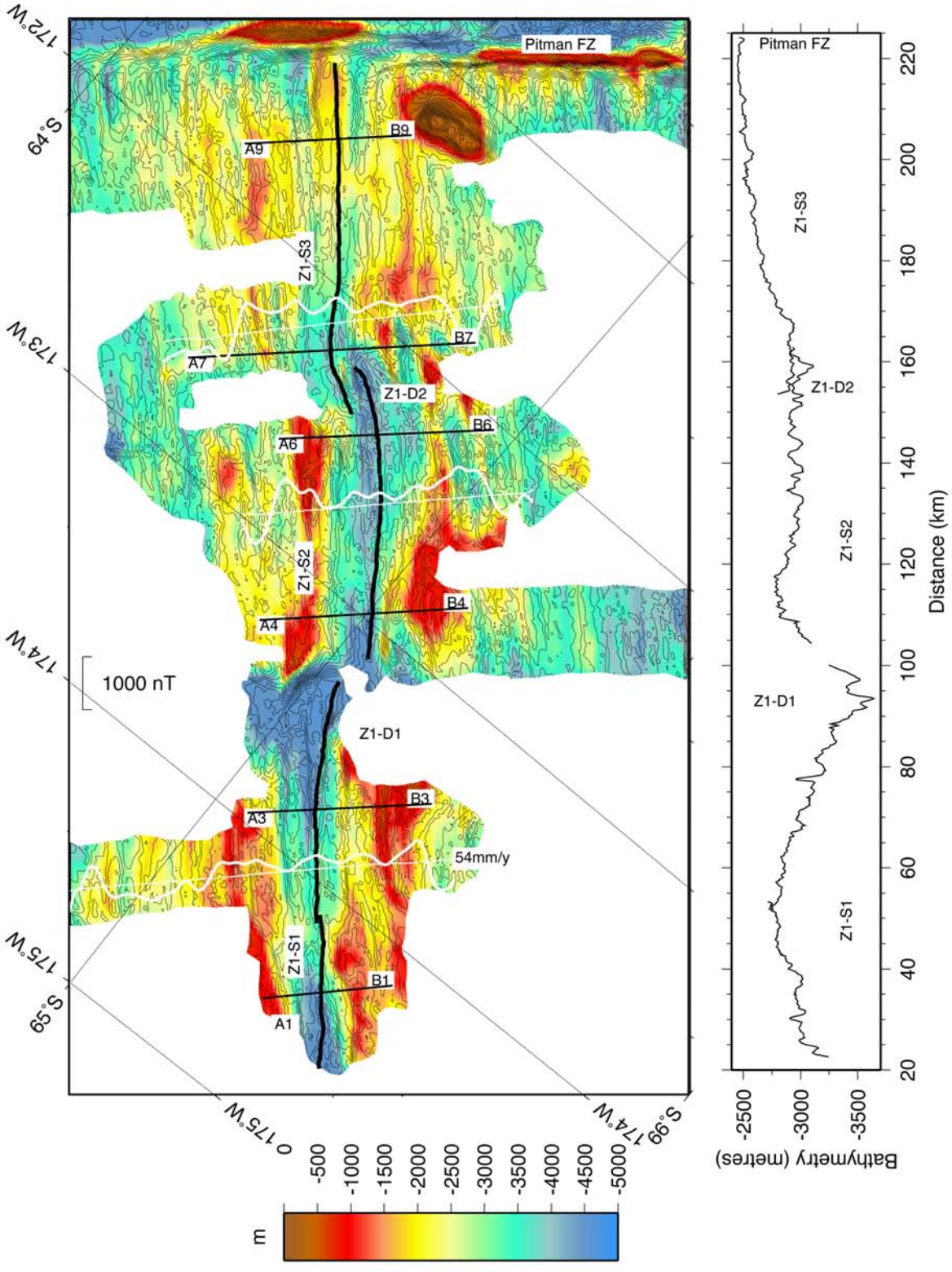

Plate 1. Top bathymetric map (100-m isocontours) of zone 1 (see inset in Figure 1b) showing discontinuities and segment names. Spreading axis is materialized by a thick black line. White wiggle lines indicate along-track magnetic data. Positive and negative magnetic anomalies are respectively above and below thin white line. Bathymetric cross sections (thin black lines) are shown in Figure 2. Full spreading rate is indicated. Bottom axial depth expressed versus distance from an arbitrary, southern point located at the Pacific Antarctic Ridge/Erebus FZ intersection, near 65°58'S, 175°W.

Both discontinuities (D1 and D2) are very much alike, shaping a rift/rift overlaping spreading center (OSC) type structure. The only other documented example of such an OSC linking two segments having both an axial rift valley is in the Central Indian Ridge near 21°40'S, 69°E [*Briais*, 1995]. The observed wrapped structures may result from changes in plate geometry [*Lonsdale*, 1994b], rather than the relative progression of the magma supply below one segment [*Macdonald et al.*, 1986].

Table 1. Nomenclature and Geological Characteristics of Segmentation for Zone 1[a]

Segment	Segment Length, km	Strike	Axis Morphology	Width of Axial Valley or Axial High, km	Average Depth at the Axis, m	Axial Valley Depth, m	Discontinuity in the South	Discontinuity in the North
Z1-S1	> 80	N52°-N60°	valley	14	3000-3200	400-600	not mapped	OSC V/V 65°03'S/173°13'W
Z1-S2	70	N50°	valley	15-20	2800-3000	400-600	OSC V/V 65°03'S/173°13'W	OSC V/V 64°42'S/172°15'W
Z1-S3	75	N50°	valley to flat axial area	6-10	2400	200-400	OSC V/V 64°42'S/172°15'W	Pitman FZ 64°40'S/170°40'W

[a] See Plate 1 and location in Figure 1b. V/V, valley/valley; D/D, dome/dome.

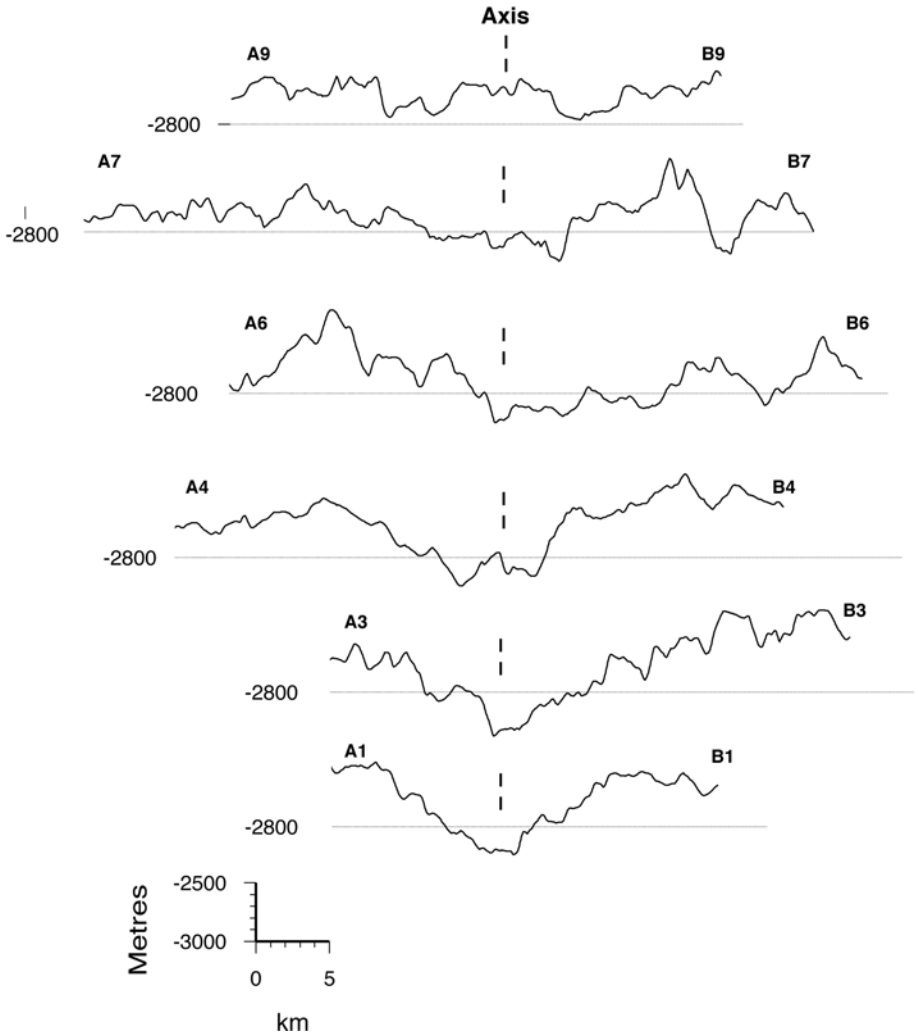

Figure 2. Cross-sectional bathymetry from zone 1 (see sections location in Plate 1). Straight, black lines indicates 2800 m below sea surface level. Spreading axis location is materialized by dashed lines.

3.2. Zone 2: Transitional Area

In the transitional area the axial morphology is generally ill defined, has a low cross-sectional relief, and alternates between more or less pronounced rift valleys, flat areas, and axial highs (Figures 3 and 4, Table 2). The spreading rate increases between ~ 56 mm/yr near 65°S, 171°W (close to Pitman FZ), and up to 66 mm/yr near 62°S, 158°W (close to Le Renard FZ) (Figure 1b). The zone has been covered more extensively off-axis south of Heirtzler transform fault than north of it. Figures 2 and 3 present the two sections separately (Z2A, Plate 2 and Figure 3; Z2B, Plate 3 and Figure 4).

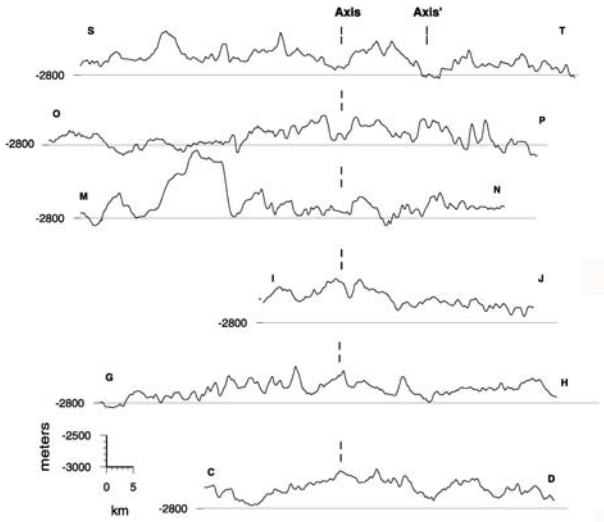

Figure 3. Cross-sectional bathymetry from zone Z2A (see sections location in Plate 2). Straight, black lines indicate 2800 m below sea surface level. Spreading axis location is materialized by dashed lines.

Discontinuities are of three types: small deviations of axial linearity, OSC evolving in linking and decapitation as described by *Macdonald* [1989], and propagators. A major propagator has its tip at 63°30'S, 167°20W and shows an offset of 40 km and an overlapping of 25 km [*Briais et al.*, 1996; *Géli et al.*, 1997]. The pseudofaults are ~ 35° oblique to the propagating ridge (PR), which implies a rate of propagation of 43 mm/yr., similar to that of other PRs [e.g., *Hey et al.*, 1986]. Extrapolating the trace of the propagator pseudofaults up to Heirtzler FZ yields an age of ~ 5 Ma for the initiation of the propagation, that is shortly after Chron 3a, which corresponds to the age of a clockwise change in spreading direction [*Cande et al.*, 1995]. A second, smaller, southward propagator (discontinuity Z2A-D4) is observed northeast of the major one at 63°15'S and 165°10'W, with a morphology similar to that of the larger one (Plate 2). The overlap is 25 km long and the offset 18 km wide. It is inferred to have started at ~ 0.8 Ma, at the time of a clockwise rotation of the spreading direction.

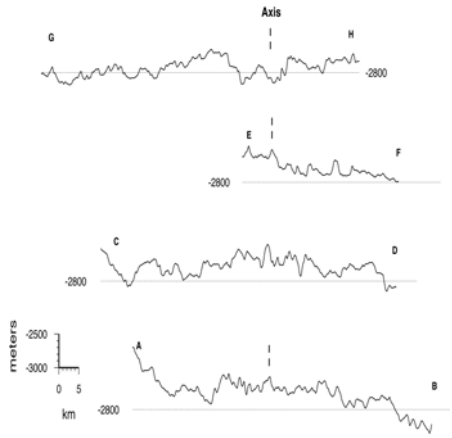

Figure 4. Cross-sectional bathymetry from zone Z2B (see sections location in Plate 3). Straight, black lines indicate 2800 m below sea surface level. Spreading axis location is indicated by dashed lines.

Northeast of Heirtzler FZ (in zone Z2B Plate 3), only two small sections of the axis have been mapped. Between Heirtzler and La Rose FZs, along and across-strike profiles exhibit a flat axial morphology (Figure 4). North of the 100-km-long, right-stepping La Rose offset, one line crossing the axis near 62°40'S, 159°30'W reveals a 15-km-wide, 300-m-deep rift valley and provides a direct estimation of the spreading rate of ~ 66 mm/yr.

Table 2. Nomenclature and Geological Characteristics of Segmentation for Zone 2A [a]

Segment	Segment Length, km	Strike	Axis Morphology	Width of Axial Valley or Axial High, km	Average Depth at the Axis, m	Axial Valley Depth, m	Discontinuity in the South	Discontinuity in the North
Z2A-S1	55	N45°	dome	12	2200	400	Pitman FZ 64°40'S/170°40'W	DEVAL 64°27'S/169°35'W
Z2A-S2	75	N45°	flat axial area	10	2300	200	Deval 64°27'S/169°35'W	OSC D/D 64°S/169°W
Z2A-S3	100	N45°	dome	8	2200	300	OSC D/D 64°S/169°W	PR1 63°45'S/167°W
Z2A-S4	150	N45°-50°	valley	6-14	2700	300-400	PR1 63°45'S/167°W	PR2 63°20'S/165°W
Z2A-S5	> 30	N45°-50°	valley	6-10	2800	500	PR2 63°20'S/165°W	Heirtzler FZ?

[a] See Plate 2 and location in Figure 1b.

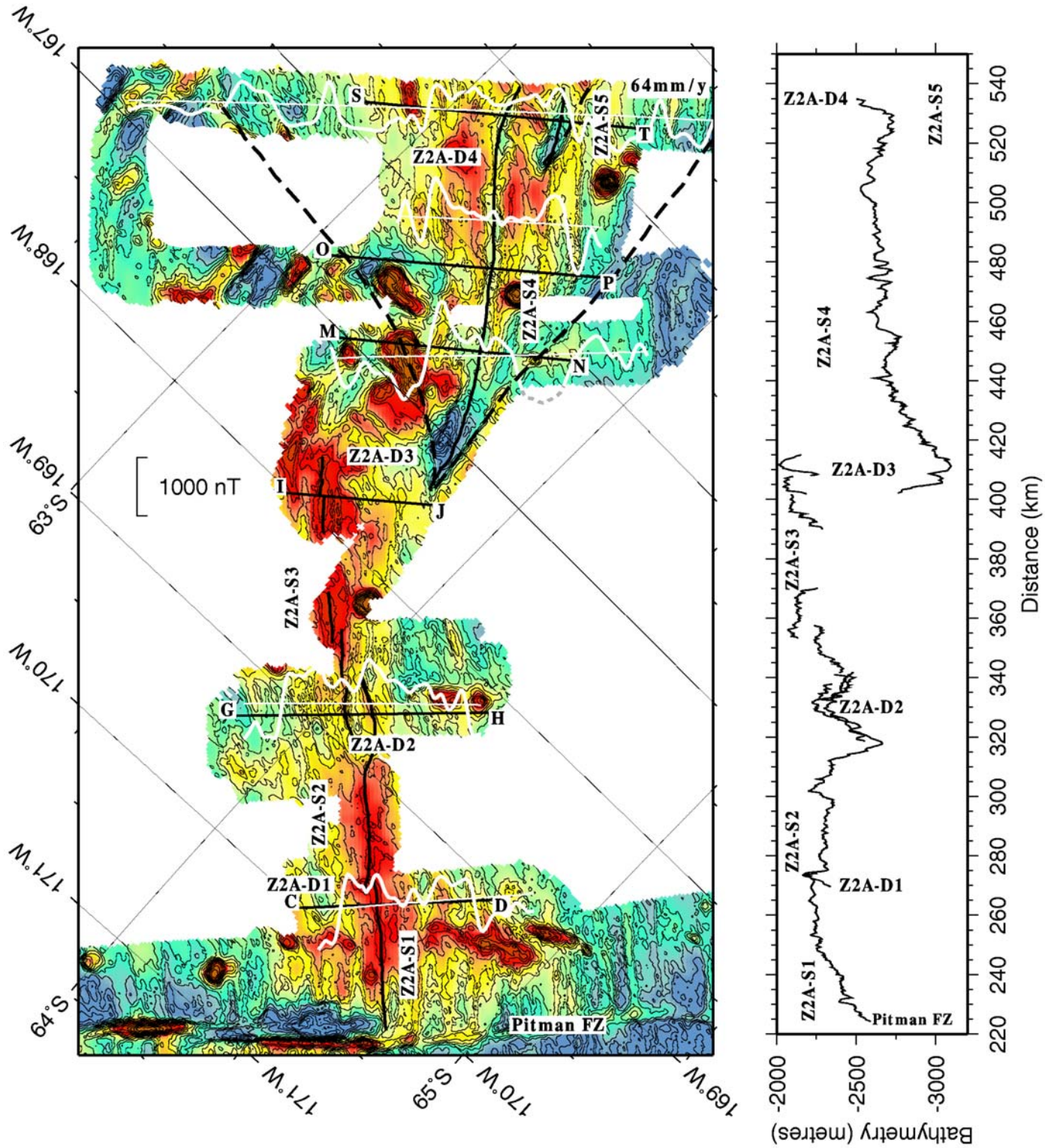

Plate 2. Top bathymetric map (100-m isocontours) of zone 2A (see inset in Figure 1b) showing discontinuities and segment names. Spreading axis is materialized by a thick black line. The outer and inner pseudofaults of the 167°W propagator are materialized by dotted lines. White wiggle lines indicate along-track magnetic data. Positive and negative magnetic anomalies are above and below, respectively, thin white line. Bathymetric cross sections (thin black lines) are shown in Figure 3. Full spreading rate is indicated. Bottom axial depth expressed versus distance from an arbitrary, southern point located at the Pacific Antarctic Ridge/Erebus FZ intersection, near 65°58'S, 175° W.

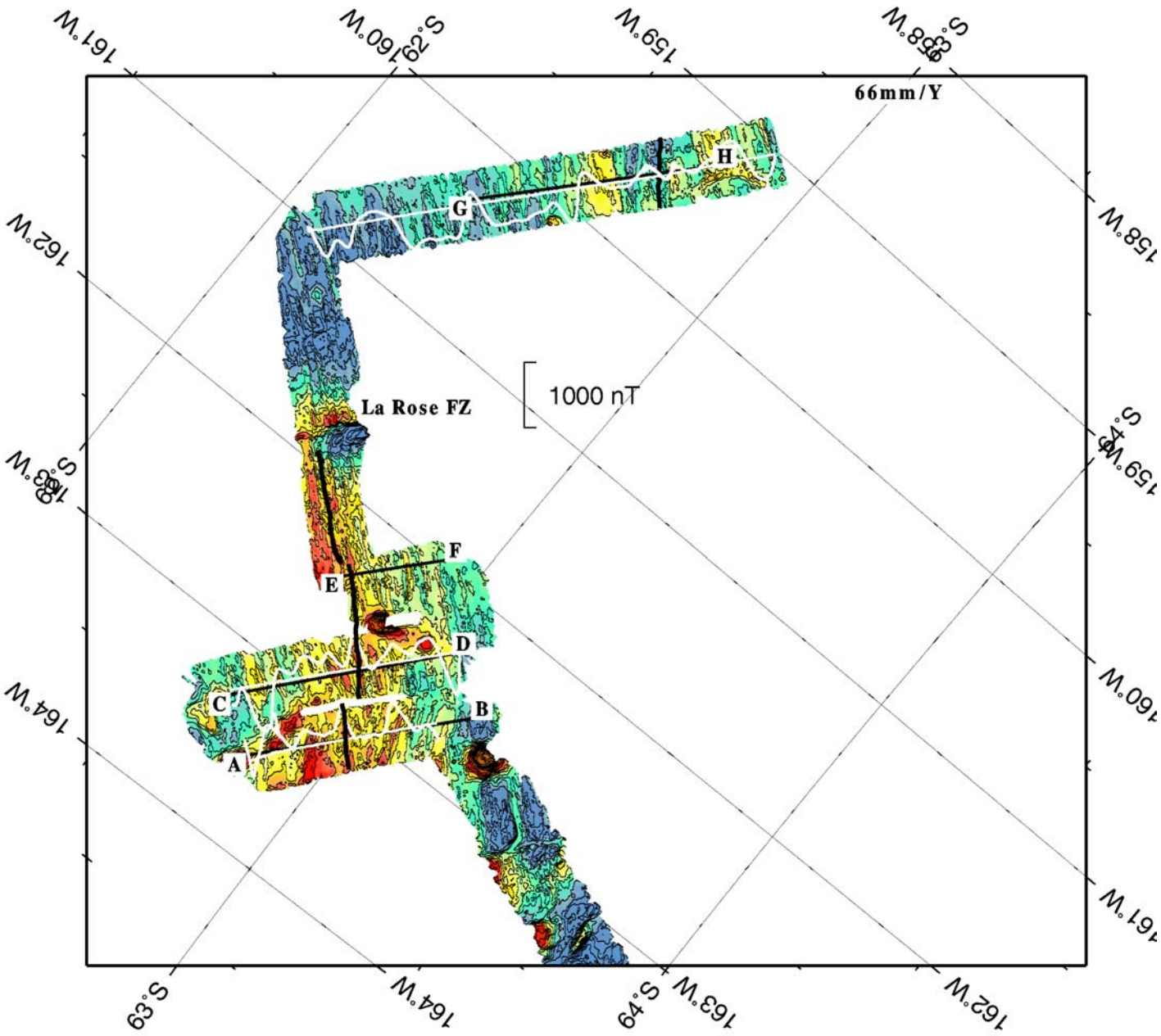

Plate 3. Bathymetric map (100-m isocontours) of zone 2B (see inset in Figure 1b) showing discontinuities and segment names. Spreading axis is materialized by a thick black line. Bathymetric cross sections (thin black lines) are shown in Figure 4. White wiggle lines indicate along-track magnetic data. Positive and negative magnetic anomalies are above and below, respectively, thin white line.

It is interesting to note that the bathymetric expression of the fossil traces of Heirtzler, La Rose, and Le Renard FZs (crossed near 63°30'S, 164°W; 62°30'S, 162°15'W; and 62°45'S, 158°30'W, respectively) are not very pronounced but are characterized by a trough that is not deeper ~ about 500 m. It is also difficult to follow the fracture zones in the satellite gravity map. Some transform faults like the Heirtzler transform fault (TF) are even characterized by a series of gravity highs, suggesting that the transform fault is presently evolving and progressively disappearing.

3.3. Zone 3: Fast Spreading Morphology

This zone extends from to 63°S, 159°W to 55°30'S, 144°W, between Le Renard and Udintsev FZs, covering an along-axis distance of 1100 km (Figure1b). It is characterized off-axis by the previously described large V-shaped structure that appears in the satellite gravity map [*Sahabi et al.*, 1996]. A gap in the mapping coverage of the axial area exists between 61°40'S, 154°W and 61°S, 153°15'W (Plate 4). South of this gap, the mapping extends off-axis up to 6 Ma, covering the expected tip of the V. North of it, only the axial rise crest has been covered, so that we have no magnetic anomaly control on the location of the spreading axis (Plate 5) but old National Geophysical Data Center (NGDC) profiles have been studied to help axis localization. According to the previous kinematics analysis including magnetic data from Pitman FZ [*Cande et al.*, 1995], the spreading rate in zone 3 varies between 68 and 76 mm/yr.

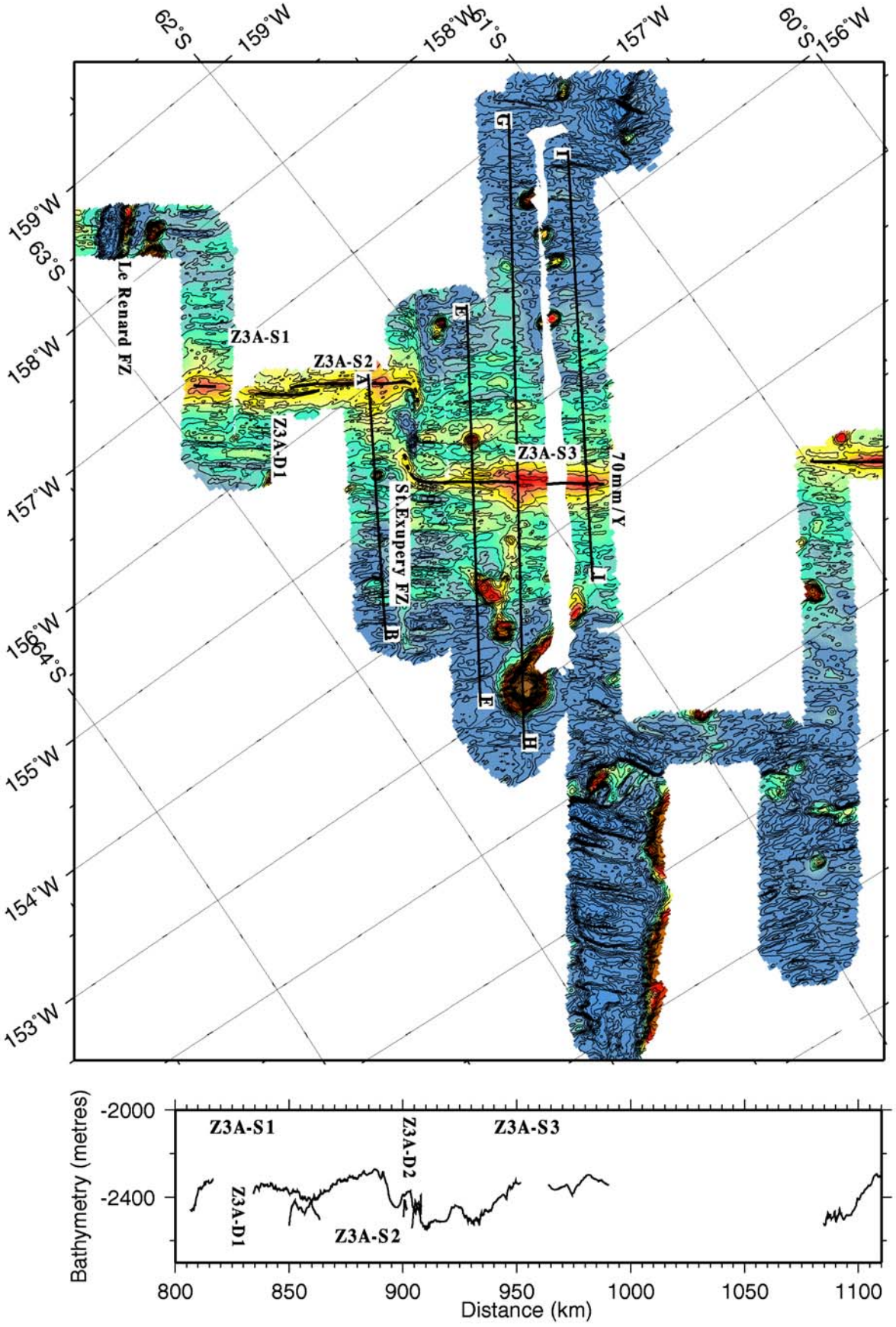

Plate 4. Top bathymetric map (100-m isocontours) of zone 3A (see inset in Figure 1b) showing discontinuities and segment names. Spreading axis is materialized by a thick black line. Dotted lines near Saint-Exupéry FZ indicate volcanic structures overshooting the transform fault. Bathymetric cross sections (thin black lines) are shown in Figure 5. Magnetic wiggles are shown in Figure 8. Full spreading rate is indicated. Bottom axial depth expressed versus distance from an arbitrary, southern point located at the Pacific Antarctic Ridge/Erebus FZ intersection, near 65°58'S, 175° W.

The main characteristic of the segmentation pattern and axial morphology is the presence of axial high at the axis, except in the close vicinity of some of the axial discontinuities. These axial highs are similar to those observed at the crest of the EPR, most particularly between Siqueiros and Rivera FZs, where the spreading rate ranges between 117 and 84 mm/yr [*Macdonald et al.*, 1992], or at the crest of the SEIR between 90°E and 100°E, where the spreading rate is ~ 80 mm/yr [*Sempéré et al.*, 1997; *Cochran et al.,* 1997]. The variations in axial morphology are systematically related to variations in axial depth and cross-sectional area (Figures 5 and 6), suggesting that the morphology is likely to be primarily controlled by along-axis variations in magma supply [e.g., *Macdonald et al.,* 1992].

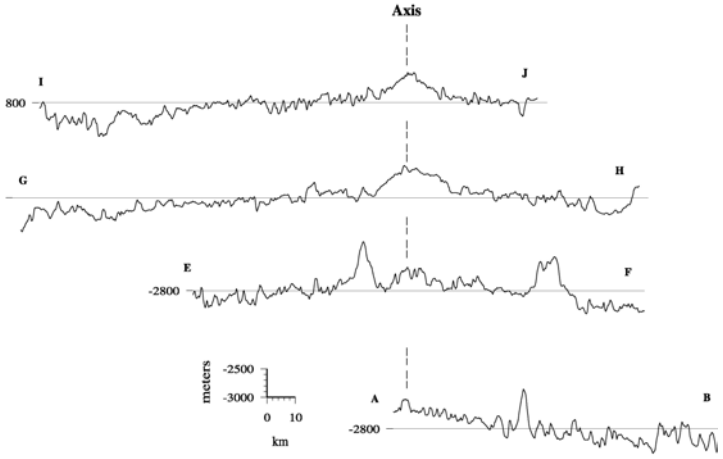

Figure 5. Cross-sectional bathymetry from zone Z3A (see sections location in Plate 4). Solid lines indicate 2800 m below sea surface level. Spreading axis location is materialized by dashed lines.

Between Le Renard and Udintsev FZs, the axis is offset by three, 50 to 80-km-long, right-stepping transform faults (Plates 4 and 5; Tables 3 and 4), namely, Saint Exupéry FZ, near 62°10'S, 155°30'W; L'Astronome FZ, near 59°30'S, 151°W; and Le Géographe FZ, near 57°35'S, 147°30'W. Three overlapping spreading centers (OSCs) located near 62°25'S, 156°15'W; 60°10'S, 152°15'W; and 58°30'S, 144°W), respectively, and one deviation of axial linearity (near 57°5'S, 146°10'W) further partition the axis into second-order segments.

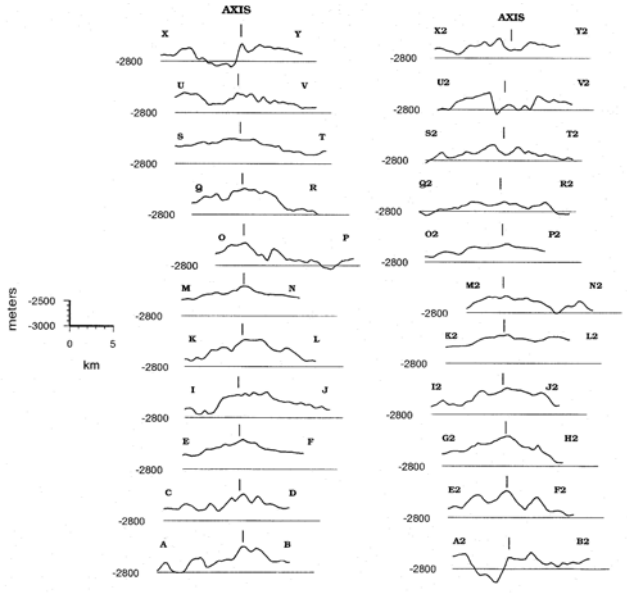

Figure 6. Cross-sectional bathymetry from zone Z3B (see section location in Plate 5). Black lines indicate 2800 m below sea surface level. Spreading axis location is shown**.**

One left-stepping OSC probably exists near 153°20'W, 61°S, but it has not been mapped.

The three, right-stepping transform faults named above are characterized by one or two 800 to 1000-m-deep, 40 to 60 km-long rhomboidal basins reaching a depth of 3500 m (Plate 6). On both ends of each transform valley, two overshot ridges are subparallel to the transform fault, wrapping over it by ~ 20 km. Here in after, we call this type of first-order discontinuity "wrapped transform fault" (WTF) [*Aslanian et al.*, 1996]. A similar bended structure was previously observed by *Lonsdale* [1994a] on the Antarctic flank of the Heezen FZ and interpreted as an "overshot ridge" resulting from changes in the relative plate motion.

The extension across the transform valley by oblique slip results in a 10-km shift of the fossil traces of the transform fault. Within the Le Géographe transform (Plate 6), an extensional structure appears as a possible incipient spreading center, recalling the initial stage of the midtransform axis that has developed in the transform valley of the Raitt FZ *Lonsdale* [1994a]. Clearly, the special shape of the WTFs, the shift between the fossil traces, and the apparent, possible incipient partition of Le Géographe transform into two smaller discontinuities may all be attributed to extension in response to Pliocene clockwise rotations of the Pacific-Antarctic spreading boundary.

Table 3. Nomenclature and Geological Characteristics of Segmentation for Zone 3A [a]

Segment	Segment Length, km	Strike	Axis Morphology	Width of Axial Valley or Axial High, km	Average Depth at the Axis, m	Axial Valley Depth, m	Discontinuity in the South	Discontinuity in the North
Z3A-S1	> 65	N40°	flat dome	4-6	2300	200	Le Renard FZ? 62°45'S/158°30'W	OSC D/D 62°30'S/156°20' W
Z3A-S2	60	N38°	dome	4-6	2300	200	OSC D/D 62°30'S/156°20'W	St Exupéry FZ 62°15'S/155°30' W
Z3A-S3	> 100	N38°	dome	5-30	2500	100-600	St Exupéry FZ 62°15'S/155°30'W	?

[a] See Plate 4 and location in Figure 1b.

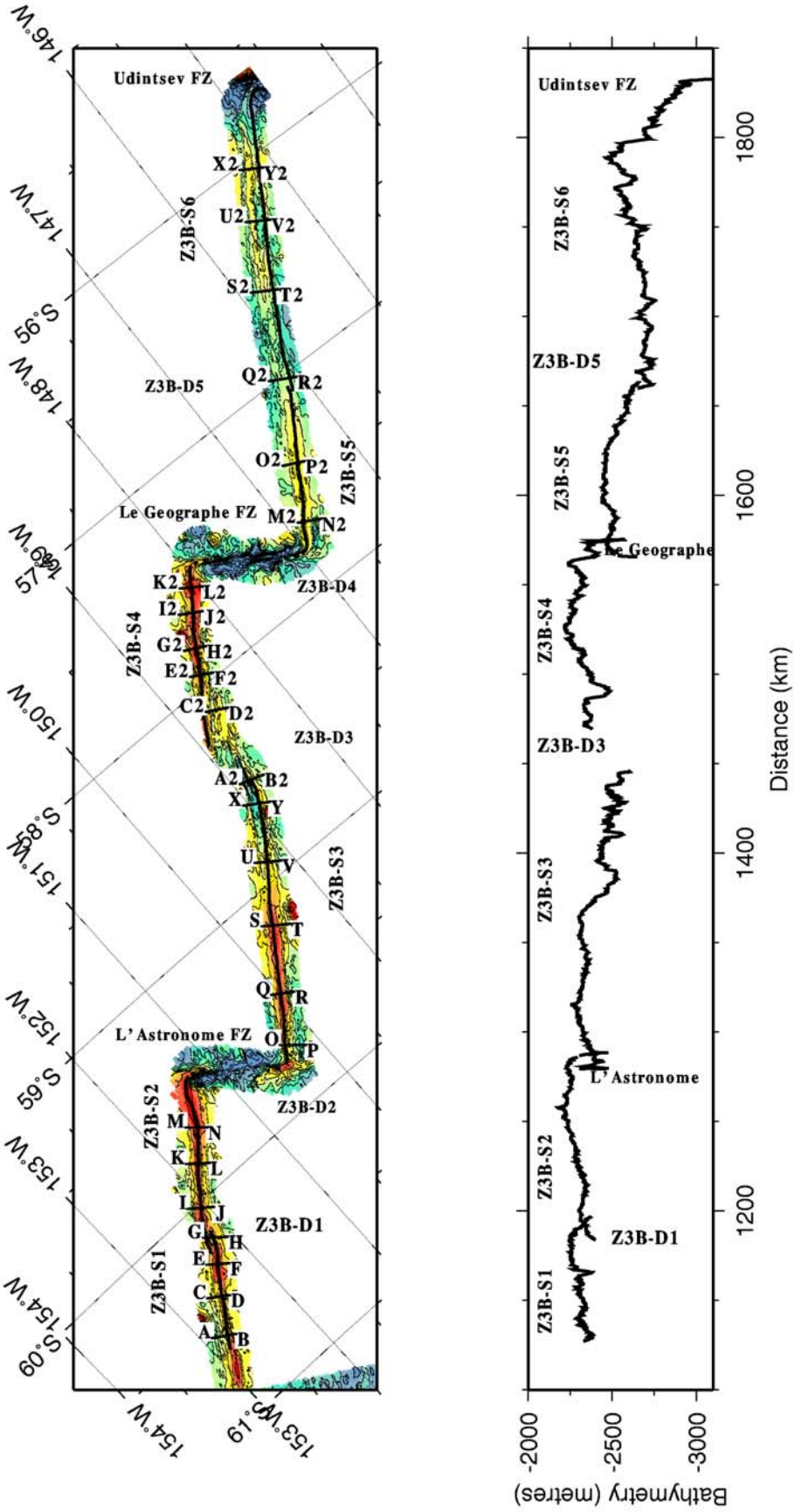

Plate 5. Top bathymetric map (100-m isocontours) of zone 3B (see inset in Figure 1b) showing discontinuities and segment names. Spreading axis is materialized by a thick black line. Dotted lines near axial transform discontinuities indicate volcanic structures overshooting the transform fault. Bathymetric cross sections (thin black lines) are shown in Figure 6. Bottom axial depth expressed versus distance from an arbitrary, southern point located at the Pacific Antarctic Ridge/Erebus FZ intersection, near 65°58'S, 175°

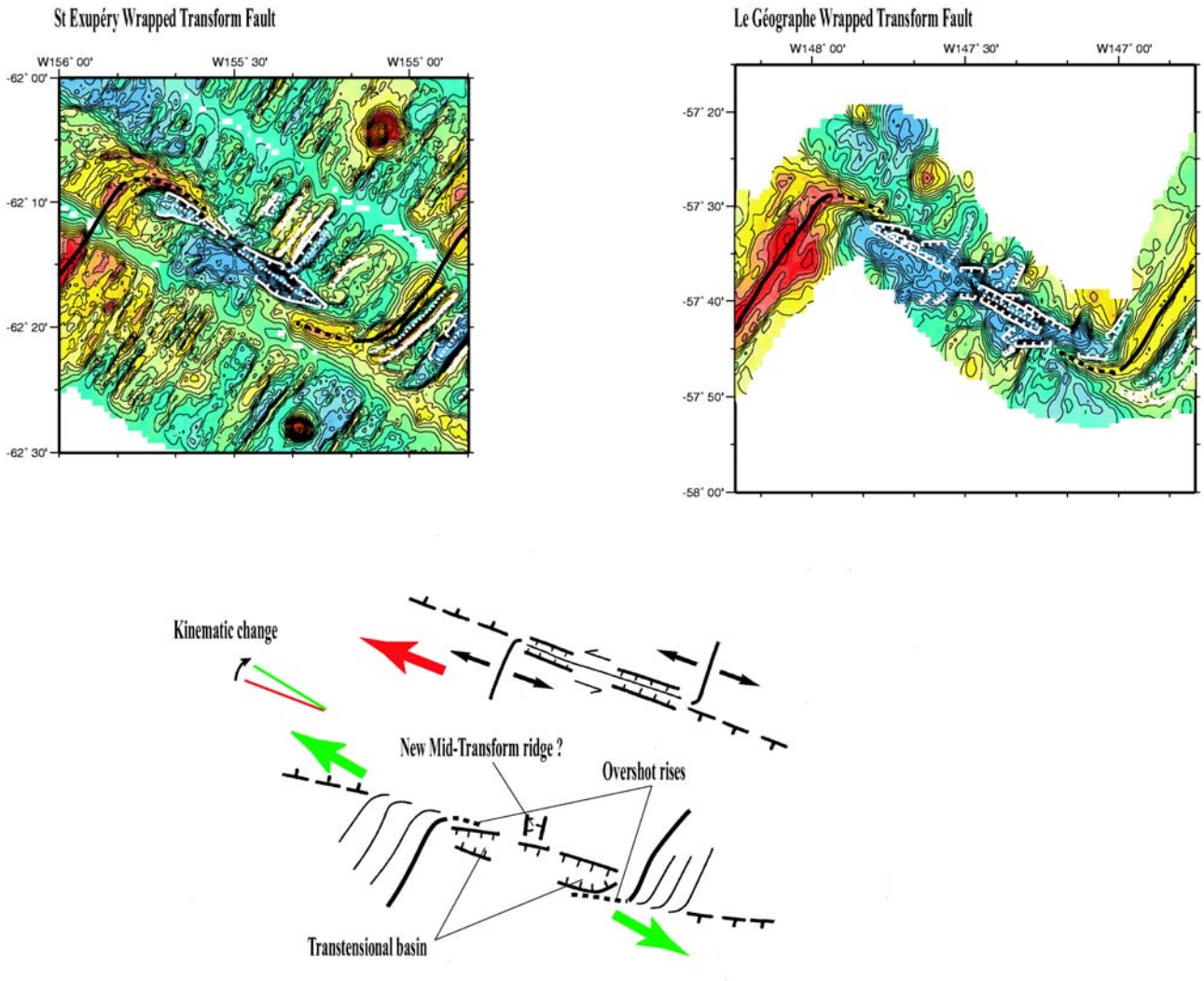

Plate 6. Focus on wrapped transform faults (WTF) and interpretative sketch. The thick black line indicates the spreading axis. White lines indicate the main structural features. Dotted lines are for depressions; small crosses are for highs. Barbed lines (with tick marks pointing downward) indicate faults. (a) Saint Exupéry WTF. This N125°E trending structure offsets the axis by 50 km. A deep 40-km-wide extensional basin, reaching 3500 m in depth, is present between the two branches of the spreading axis. These branches bend and are prolongated by overshot ridges that plunge inward, wrapping the basin. (b) Le Géographe WTF. This N123+E trending structure offsets the axis by 65 km and shows more or less rhomboidal extensional basins reaching 3250 in depth. On both ends of the transform fault (TF), the axial crest of the PAR bends and is prolongated by an overshot ridge that plunges inward. (c) Sketch showing the effect of a change in plates relative motion on the geometry of the transform offset: Kinematic changes may induce the creation of transtensional basins, as well as overshot ridges and (possibly) accretion centers within the transform fault [after *Lonsdale*, 1994a]

Table 4. Nomenclature and Geological Characteristics of Segmentation for Zone 3B [a]

Segment	Segment Length, km	Strike	Axis Morphology	Width of Axial Valley or Axial High, km	Average Depth at the Axis, m	Axial Valley Depth, m	Discontinuity in the South	Discontinuity in the North
Z3B-S1	> 120	N35°	dome	4-6	2300	300	?	OSC D/D 60°12'S/152°15'W
Z3B-S2	110	N34°	dome	4-7	2200	200	OSC D/D 60°12'S/152°15'W	L'Astronome FZ 59°40'S/150°50'w
Z3B-S3	180	N33°	dome	4-6	2300	100-300	L'Astronome FZ 59°40'S/150°50'w	OSC? 58°30'S/149°20'W
Z3B-S4	> 120	N32°	dome	4-10	2300	200-400	OSC? 58°30'S/149°20'W	Geographe FZ 57°40'S/147°30'W
Z3B-S5	110	N31°	dome	8-10	2400	200-300	Geographe FZ 57°40'S/147°30'W	Deval 57°05'S/146°12'W
Z3B-S6	180	N30°	valley	2-5	2700	200-400	Deval 57°05'S/146°12'W	Udintsev FZ

[a] See Plate 5 and location in Figure 1b.

4. Off-Axis Observations at the Tip of the V-Shaped Structure

Shipboard observations collected off-axis at the tip of the large V-shaped structure help to decipher the evolution of the plate boundary in the northern area in response to changes in the relative plate motion. Inside the V-shaped structure (for crust produced after Chron 2a) the seafloor topography is smooth and abyssal hills are parallel to the present-day ridge axis (Figure 7a). On crust older than ~ 3 Ma, outside the V, the abyssal hill tips are bended inward. South of the bathymetric coverage, on the Antarctic flank, satellite gravity data indicate the presence of a fracture zone (named Le Petit Prince FZ), which disappears on crust younger than ~ 4.5 to 5 Ma. Near 152°W, 62°30'S, a complex structure is imprinted on 3-to 4-Myr-old seafloor. Two bended valleys that are more or less parallel to the axis and about 40 km long and 35 km apart limit this structure. Between the two valleys, there is a zone of ridges oriented NNE, oblique to the local trend of the abyssal hills or fracture zones. Prior to Chron 3a, Le Petit Prince FZ was a right-stepping offset of the PAR axis. As the spreading direction rotated clockwise [*Cande et al.*, 1995], the transform offset decreased, and the transform turned into a giant overlapping spreading center (GOSC).

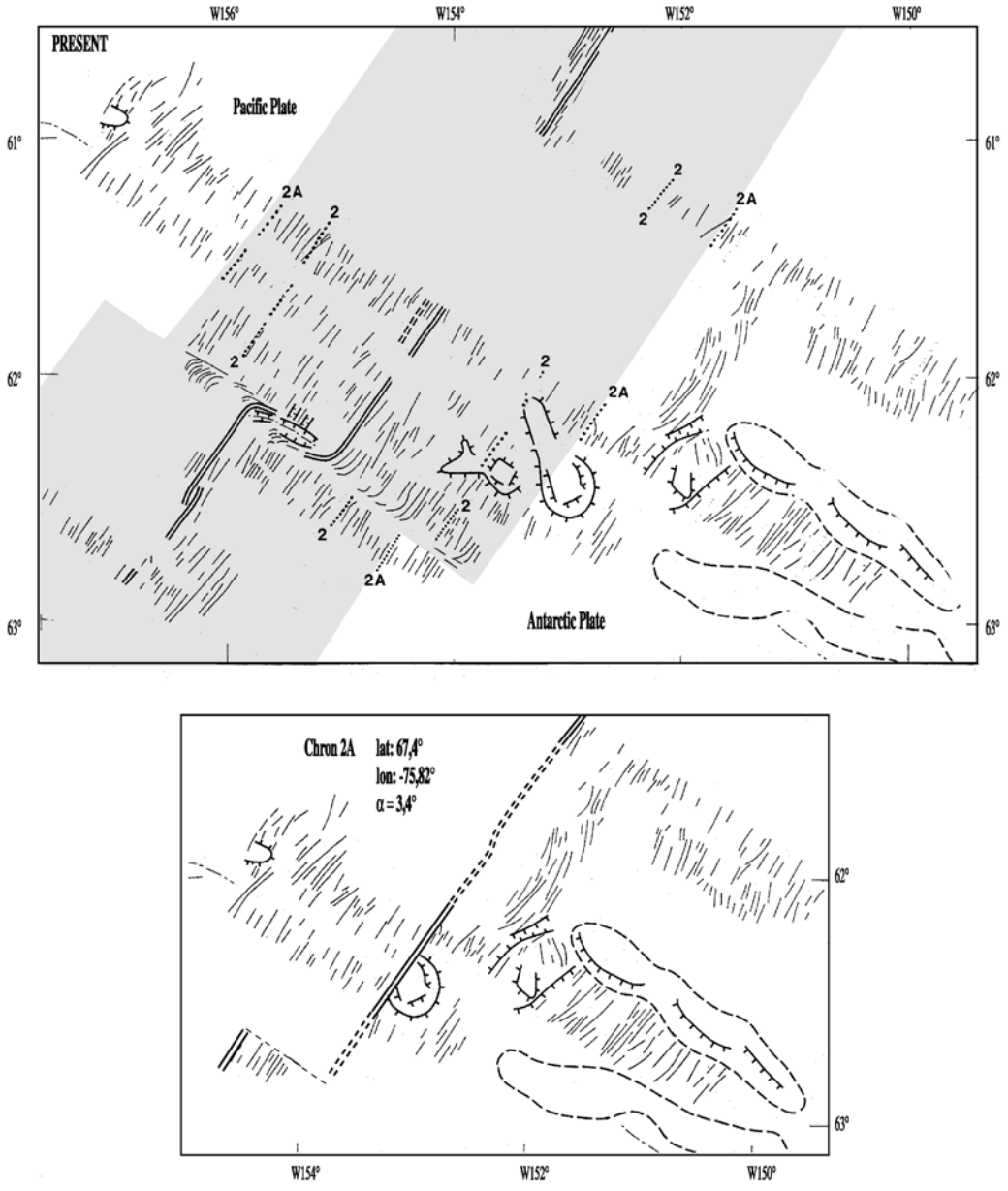

Figure 7. Evolution of Saint-Exupéry FZ. Double line is present-day spreading axis (solid, inferred from R/V *L'Atalante*'s data; dashed, inferred from satellite gravity data). Thin lines are lineations. Barbed lines correspond to the main scarp (with tick marks pointing downward), and dashed lines delineate positive gravity highs inferred from satellite derived gravity data. (a) Present-day situation. Magnetic Chrons 2 and 2a are based on the interpretation of magnetic anomalies shown in Figure 8 (dots indicate the main magnetic anomaly peak). Note that the structural trends are bended before Chron 2a. Shaded area represents crust younger than Chron 2ay (this area is removed in Figure 7b. (b) Situation at Chron 2ay obtained by rotating the structures younger than Chron 2ay using Euler rotations poles listed in Table 5 [after *Cande et al.*, 1995].

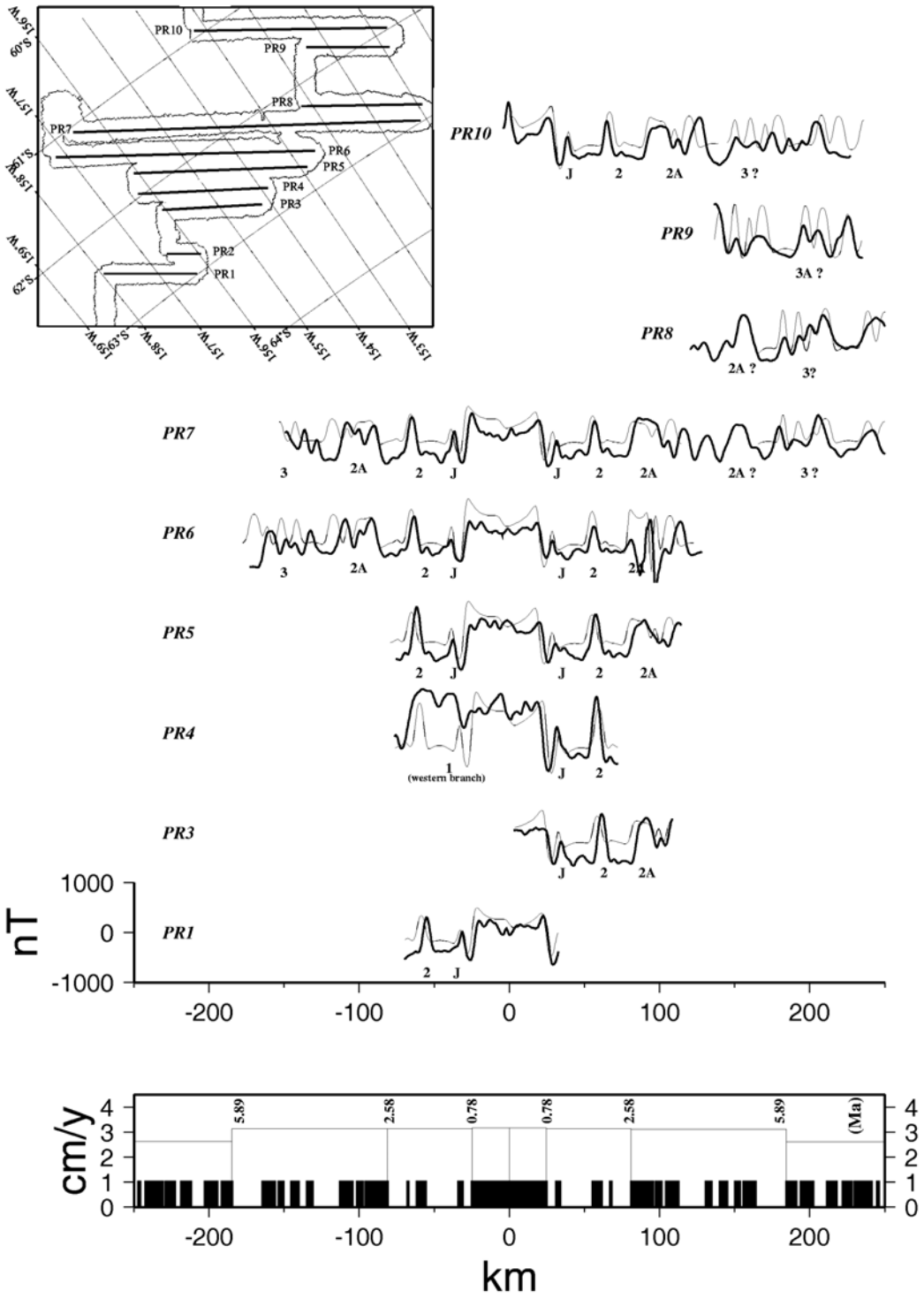

Figure 8. (opposite) Interpretation of magnetic data collected with R/V *L'Atalante* during the *Pacantarctic* cruise (see inset for profiles location, PR1 to PR10). (bottom) Scale of magnetic versus distance from the ridge axis, based on the magnetic chronostratigraphic scale of *Cande and Kent* [1995]. Spreading rates (cm/yr) versus distance to the axis are also indicated. The correspondence between distance and ages is provided by the age (vertical numbers, in Ma) dating each change in spreading rate documented by *Cande et al.* [1995]: 0.78, 2.58, 5.89 Ma, respectively. (top) Modeling (thin line) of the magnetic data (thick line), using spreading rates based on the kinematic parameters (Euler poles and rotation angles) of *Cande et al.* [1995] The zero origin on the x axis for each different profile corresponds to the location of the spreading axis. On PR 7 and PR8, the computed magnetic anomalies for ages older than ~ 3 Ma have been shifted by 45 km to the west in order to account for the presence of a vanished offset that existed prior to Chron 2a. On PR8 the shift is of a 5 km to the west (see interruption of thin line). The identification of Anomalies 1, 2, and 2a (younger part) is straightforward. Anomalies that are not unquestionally identified are indicated with a question mark. Profile PR4 crosses the spreading center two times, west and east of the Saint Exupéry wrapped transform faults, producing a perturbed central magnetic anomaly. On PR7 and PR8, the younger wiggle of Anomaly 2a appears to be duplicated on the Antarctic flank, probably because these profiles cross the two branches of the fossil giant overlapping center near 152°W, 62°30'S. On PR9, there are two wiggles that can be identified as characteristic of Anomaly 3A, assuming that a left stepping transform fault existed between profiles 8 and 9 prior Chron 3a

Between Chrons 3a and 2a (Figure 7b), the structures between the two accreting limbs of the GOSC were sheared and rotated. Then, accretion progressively stopped along the eastern branch of the GOSC, and its south-western branch linked with the northern one, leaving the fossil trace of the GOSC on the Antarctic plate. The linkage of the axis seems to have been fully completed shortly after Chron 2a. Since that time, the ridge crest has been almost continuous between 62°20'S and 59°30'S and characterized by an axial dome.

The present scenario is widely supported by the pattern of magnetic anomalies (Figure 8). Chrons J, 2, and the young part of 2A can be easily and consistently picked throughout all different across-strike profiles (Z4PR1 to Z4PR10). For ages older than ~ 3 Ma, however, the magnetic anomalies cannot always be easily matched by synthetic models simply based on the opening rates of *Cande et al.*, [1995]. For example, profile PR7 is better matched using a synthetic profile involving a small axial jump at the time of the old part of Anomaly 2A. On this profile, two peaks related to the youngest arch of magnetic Anomaly 2A are present on the Antarctic flank, while on the Pacific flank the three arches of Anomaly 2A are much narrower than expected. Along profiles PR7 and PR8, the four wiggles characteristic of Anomaly 3 are visible but shifted by as much as ~ 50 km relative to a simple magnetic model, a pattern compatible with the generation of these magnetic anomalies at the eastern branch of a vanished offset.

This supports the hypothesis that a giant overlapping spreading center (GOSC) was present with two active branches prior to Chron 2A; this GOSC evolved and finally vanished during Chron 2A, as suggested by *Géli et al.*, [1997]. Along profile PR9, two wiggles characteristic of Anomaly 3A seem to appear (Figure 8). If these two wiggles can be identified as such, then the consistency between PR8 and PR9 can be obtained by assuming that a left stepping transform offset of about 55 km was present between the two profiles (PR8 and PR9) prior to Anomaly 3A. In response to clockwise rotations of the spreading direction this transform offset progressively evolved into a giant overlapping center and off-axis reliefs formed (these reliefs are clearly visible as a series of topographic highs, presently located near 62°30'S, 152°W and oriented in the N125° direction) (Plate 4). The presence of a complete, undisturbed series of magnetic anomalies (J, 2, 2A, and 3) along profile PR10 suggests that the evolution of the transform offset was most probably fully achieved at about the time of Chron 3.

5. Evolution of Seafloor Roughness and Axial Geometry Since 35 Ma

In sections 2-4, on the basis of shipboard data we have described the evolution of the axial morphology south of Udintsev FZ and the evolution of the rough/smooth boundary near the tip of the large V. In this section, we extrapolate these results as ground truth for interpreting satellite observations. First, we analyzed the seafloor roughness using gravity and gravity slopes deduced from 1-min grids (D. Sandwell, personal communication, 2000) (Figure 9) and old bathymetric profiles (Figure 10).

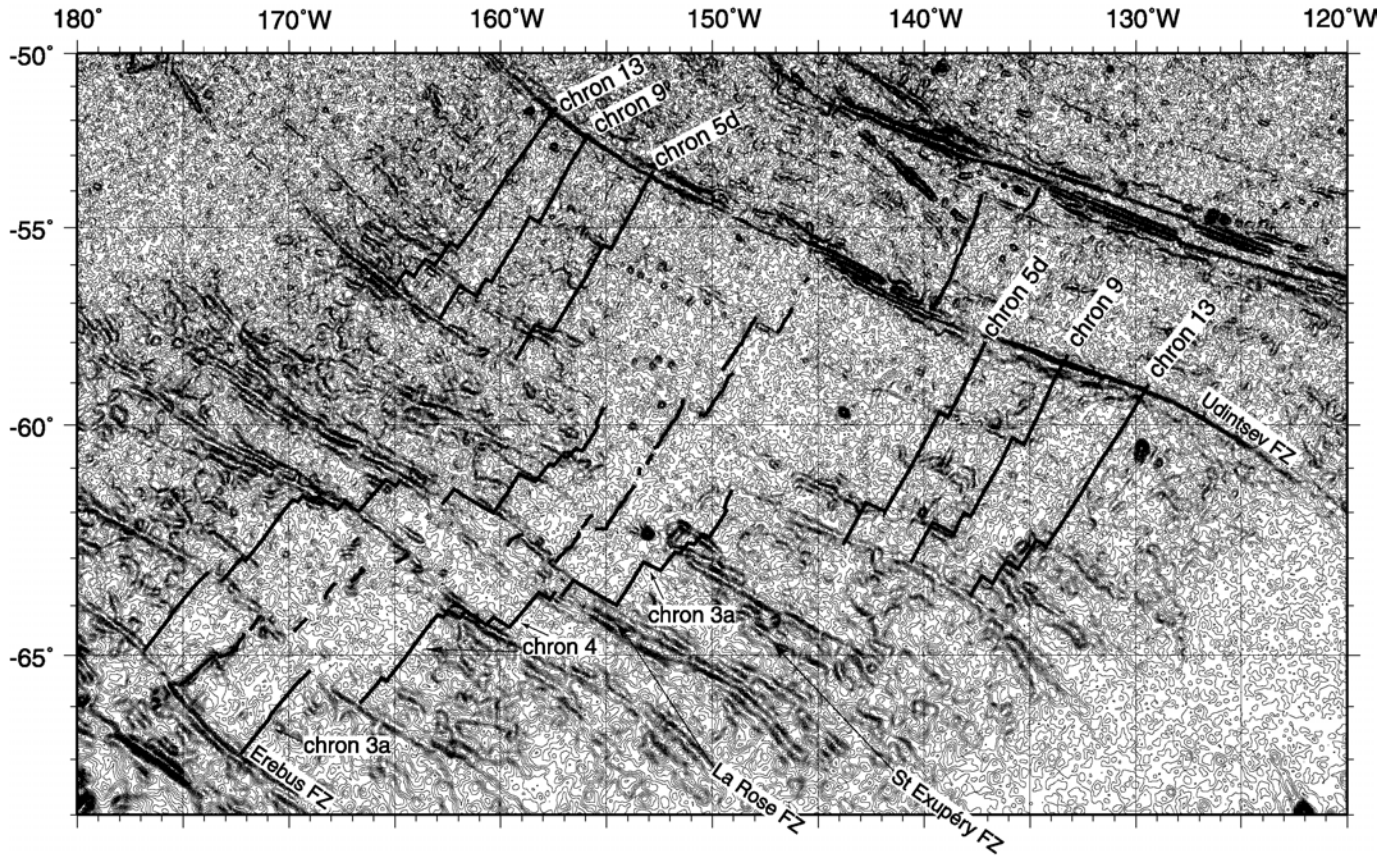

Figure 9. Isocontoured (5 mGal), high-resolution (1-min grid, courtesy of D. Sandwell), satellite-derived gravity map of the study area. Only those isochrons that appear to correspond to changes in seafloor roughness are indicated. Note that the rough/smooth transition occurs shortly after Chron 3a in the area centered on Saint Exupéry FZ and at Chron 4 between La Rose FZ and Pitman FZ.

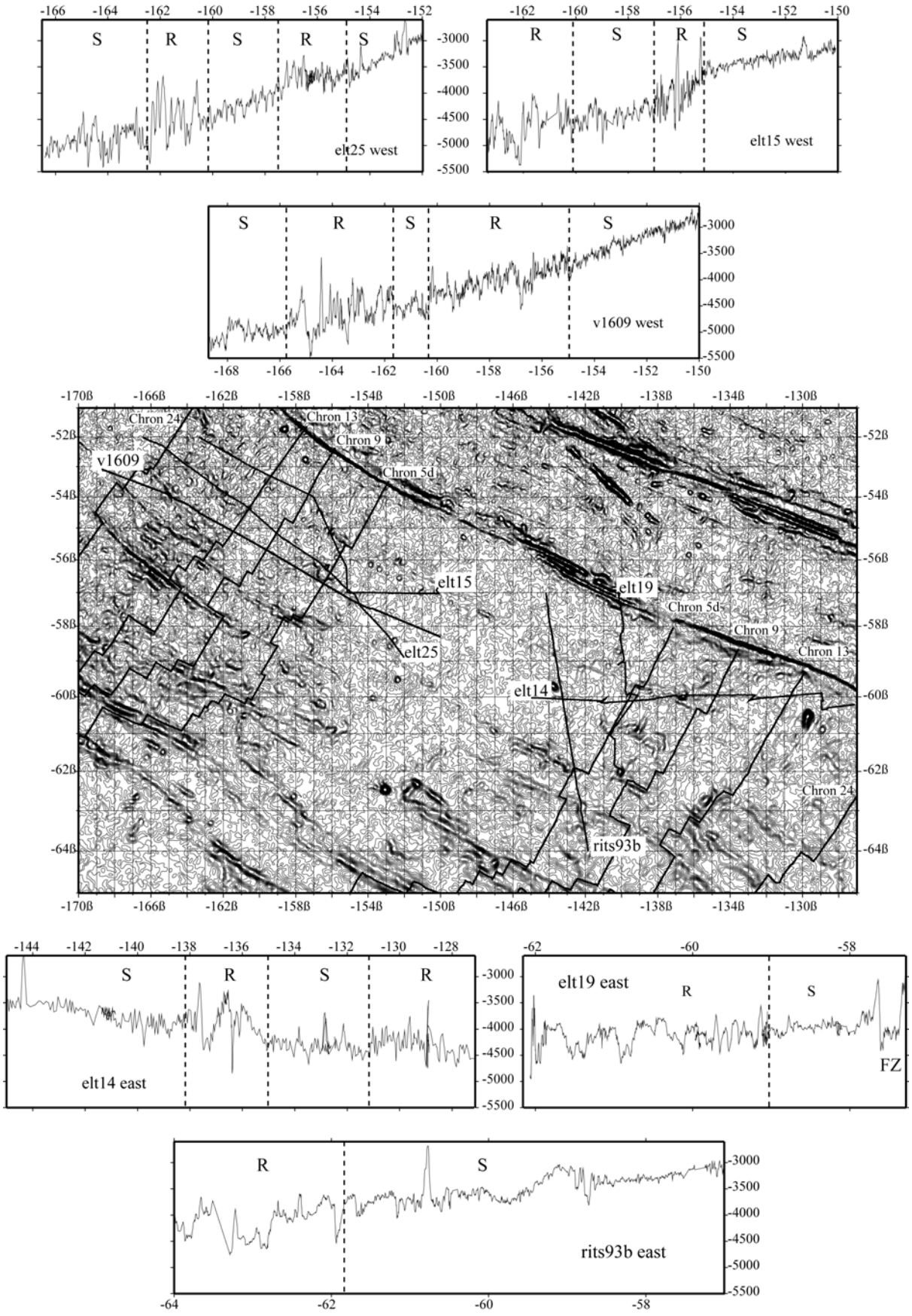

Figure 10. Comparison between the rough/smooth boundary inferred from the contoured, high resolution gravity map and the boundary inferred from actual bathymetric profiles. In total, Six ship's tracks are shown: Three on the western flank of the ridge (elt25, elt15, and v1609) and three on the eastern flank (elt14, elt19, and rits93b). Along each line, there is an alternance of rough (R) and smooth (S) seafloor domains (rough and smooth seafloor are visually characterized by respectively high and small amplitude bathymetric variations). Note the good correspondence with the rough/smooth boundary inferred from satellite-derived gravity data

.

Then by rotating all available magnetic anomaly picks (S.C. Cande, personal communication, 2000) with the Euler poles of *Cande et al.* [1995] (Table 5) for identifying the trace of fracture zones, we have reconstructed the geometry of the isochrons (Plate 7). Therefore we were able to follow the evolution of the rough/smooth transition at different epochs during the last 35 Myr (at Chrons 2ay, 3ay, 4, 5d, 9, and 13y, respectively). The different following steps can be described (Plate 8):

1. Before Chron 13y (Plate 8a), the spreading rate south of Udintsev FZ is everywhere >50 mm/yr (full rate), and all the area is rough.
2. Between Chrons 13y and 9 (Plate 8b), the spreading rate increases. The PAR is divided in two sections: Section 1 is north of Antipodes FZ, where the spreading rate becomes progressively <50 mm/yr. The seafloor becomes smooth as the spreading rate increases to over 50 mm/yr (yellow area in Plate 8b). Two fracture zones disappear (see circle in Plate 8b). Rift propagation (blue area) initiates at Udintsev FZ around Chron 13 and stops at Chron 9; the tip of the PR abuts against the newly formed Le Géographe FZ (see square in Plate 8b). A 260-km-long, oblique feature near 59°40'S, 133°W on the Antarctic flank and an outer pseudo-fault clearly visible near 62°S, 163°W on the Pacific flank represent the traces left on the seafloor by this fossil PR. Section 2 is south of Antipodes FZ, where the seafloor is everywhere slower than 50 mm/yr. The seafloor remains rough.
3. Between Chrons 9 and 5d (Plate 8c), the spreading rate decreases below 50 mm/yr, over the entire area south of Udintsev FZ. The seafloor roughness changes from smooth to rough north of Antipodes FZ and remains rough everywhere south of the fracture zone. The previously described propagating rifts stop, synchronously with a change in seafloor roughness. The two parts of an enigmatic relief (green area in Plate 8c) appear symmetrically on both flanks of the plate boundary, perpendicular to its strike (the fossil traces of these features are presently visible near 56°S, 157°W on the Pacific Plate and near 61°S, 139°W on the Antarctic Plate).
4. Between Chrons 5d and 4 (Plate 8d), the spreading rate increases. The PAR is again divided in two sections: Section 1 is north of Antipodes FZ, where the spreading rate is >50 mm/yr and the seafloor becomes progressively smooth (yellow area in Plate 8d). The enigmatic relief initiated after Chron 9 is rifted apart on both flanks of the plate boundary (black dots in Plate 8d). Instead, two new propagating rifts initiate after Chron 5d south of Udintsev FZ and south of L'Astronome FZ, respectively (blue area in Plate 8d). At Chron 4 these propagators stop and abut against Le Géographe FZ and Antipodes FZ, respectively. Section 2 is south of Antipodes FZ, where seafloor remains rough. An enigmatic structure develops symmetrically on both flanks of the PAR between Le Renard and Saint Exupéry FZ (green area in Plate 8d).
5. Between Chrons 4 and 3a (Plate 8e), seafloor spreading increases. Four domains of different seafloor roughness appear: (1) north of Antipodes FZ, the seafloor is smooth; (2) between Antipodes FZ and La Rose FZ, the seafloor is rough although the spreading rate is >50 mm/yr; (3) between La Rose FZ and Pitman FZ, the seafloor becomes smooth progressively, as soon as the spreading rate is >50 mm/yr; and (4) south of Pitman FZ, the seafloor is rough as the spreading rate is slower than 50 mm/yr.
6. After Chron 3a (Plate 8f), the seafloor becomes smooth everywhere. Note that between Antipodes FZ and La Rose FZ, the change in seafloor roughness only occurs when the spreading rate exceeds 62 mm/yr. Le Petit Prince FZ migrates into a GOSC (see section 4). A propagating rift initiates (blue area in Plate 8) at Antipodes FZ, resulting in the disappearance of this transform fault. A second propagator also initiates south of Heirtzler FZ in response to changes in spreading directions (see section 3). Although the seafloor is smooth all over the area, an axial valley is present south of Pitman FZ and in some places of the transitional area (see section 3), suggesting that there is not a simple correspondence between seafloor roughness and axial morphology.

The present analysis indicates that the PAR is divided into three ~700-km-long sections with different threshold spreading rates between the rough/smooth transition: north of Antipodes FZ and south La Rose FZ, the rough to smooth transition occurs when the spreading rate is greater than 50 mm/yr; in between Antipodes FZ and La Rose FZ, the change in seafloor roughness occurs only when the spreading rate is faster than 60 to 65 mm/yr. When the seafloor roughness changes from rough to smooth, propagators develop, suggesting that when the rheology is unstable, kinematics changes are likely to produce propagating rifts.

Table 5. Euler Poles of Rotation Used for Pacific and Antarctic Plate Relative Motions wiith Fixed Pacific Plate [a]

Chrons	Latitude	Longitude	Angle, deg
2ay	67.03	- 73.72	- 2.42
3ay	67.91	- 77.93	- 5.42
4	69.68	- 77.06	- 7.15
5d	73.68	- 69.85	- 15.17
9	74.38	- 69.79	- 21.61
13y	74.38	- 64.74	- 27.34

[a] Poles (except for Chron 9) are from *Cande et al.* [1995]. Pole for Chron 9 is from *Tebbens and Cande* [1997].

6. Effects of Spreading Rate on Axial Morphology and Seafloor Roughness

The spreading rate is clearly the first-order, key parameter that governs the observed transition in axial morphology (from an axial valley in the southwestern end to an axial high in the northeastern and of our study area) and the observed changes in seafloor roughness since 35 Ma. However, changes in seafloor roughness do not follow exactly the same spreading rate dependence as changes in axial morphology [*Small and Sandwell*, 1992; *Small*, 1994]. For instance, an axial valley is present south of Pitman FZ and in some places in the transitional area, while seafloor is smooth for crustal ages younger than 5 to 6 Ma. This suggests that abyssal hills generated at axial highs always result in smooth seafloor.

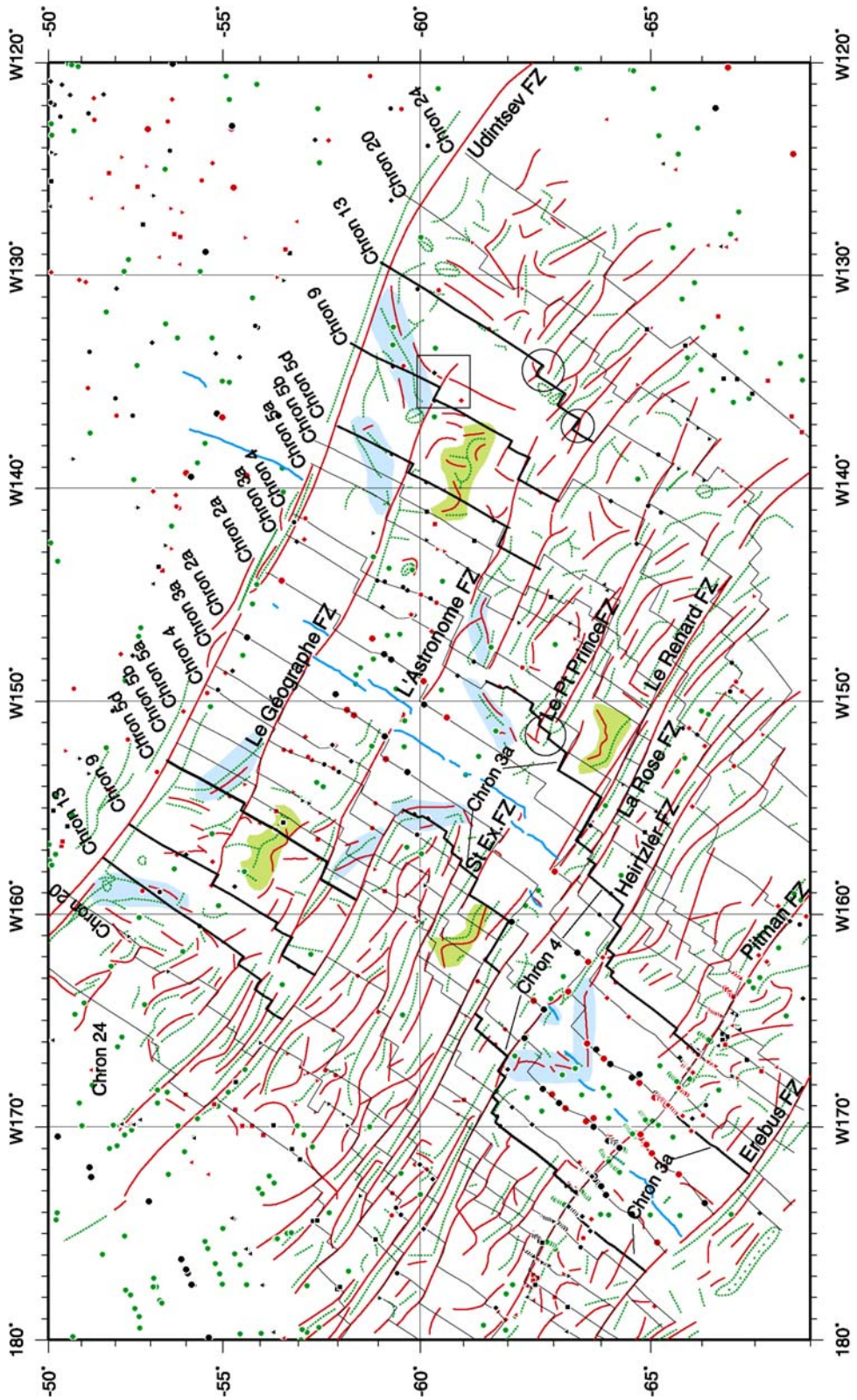

Plate 7. Synoptic sketch of the present-day, tectonic situation. Major structural features south of Udintsev FZ are based on the 1-min satellite gravity grid (D. Sandwell, personal communication, 2000) and on the one minute satellite gravity slopes grid. Red lines indicate gravity lows (e.g. fracture zones). Green, dotted lines are for gravity highs. Blue thick line is for spreading center. Blue areas represent trails of propagating rifts, fossil or present. Green areas represent trails of enigmatic structures that appear as gravity lineations, symmetrically relative to the spreading center. All available magnetic anomaly picks are represented by small black and green symbols (*S.C. Cande,* personal communication, 2000). For selected anomalies the picks (black symbols) have been rotated using the Euler poles (see Table 5) of *Cande et al.* [1995]. Rotated picks are in red. Isochrons (black lines) are based on both the actual and rotated anomaly picks, and on the direction of fracture zones. Thick isochrons approximately date transitions in seafloor roughness. Circles on the Antarctic plate focus on interruptions of fracture zones. Square focuses on the initiation of Le Géographe FZ.

.

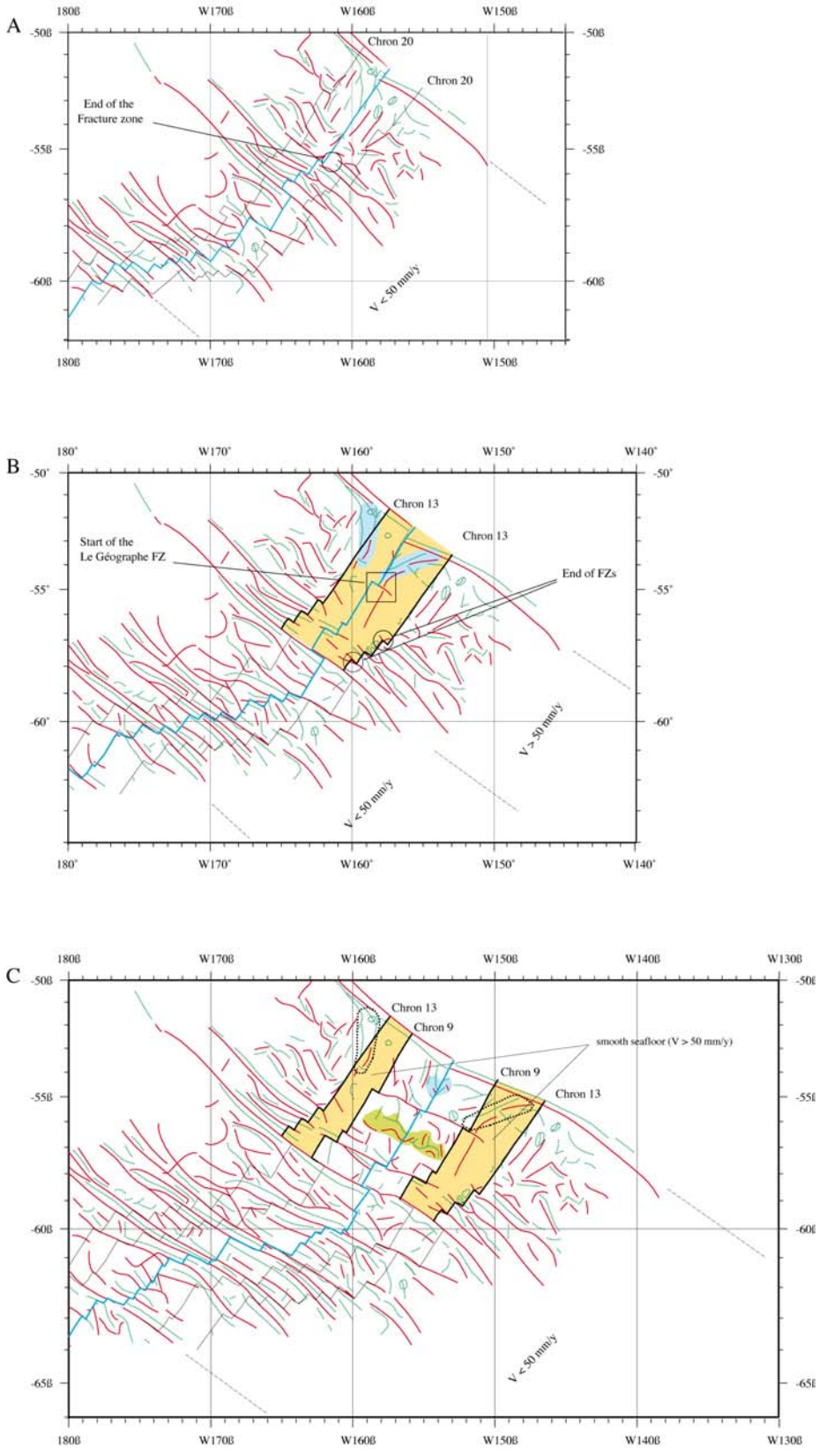

Plate 8. Kinematic reconstructions (based on the Euler poles of *Cande et al.* [1995]: see Table 5) at different, selected chrons: (a) chron 13y; (b) chron 9; (c) chron 5; (d) chron 4; (e) chron 3ay, and (f) chron 2ay. For description of structural features, see caption of Plate 7. Blue areas indicate symmetric structures that initiate at the time of the given chron. Black, dotted lines indicate contour of structures that already exist. Areas of smooth seafloor are in yellow. Interruption and initiation of fractures are indicated by circles and squares, respectively. V is full spreading rate averaged for the period comprised between the given chron and the previous one.

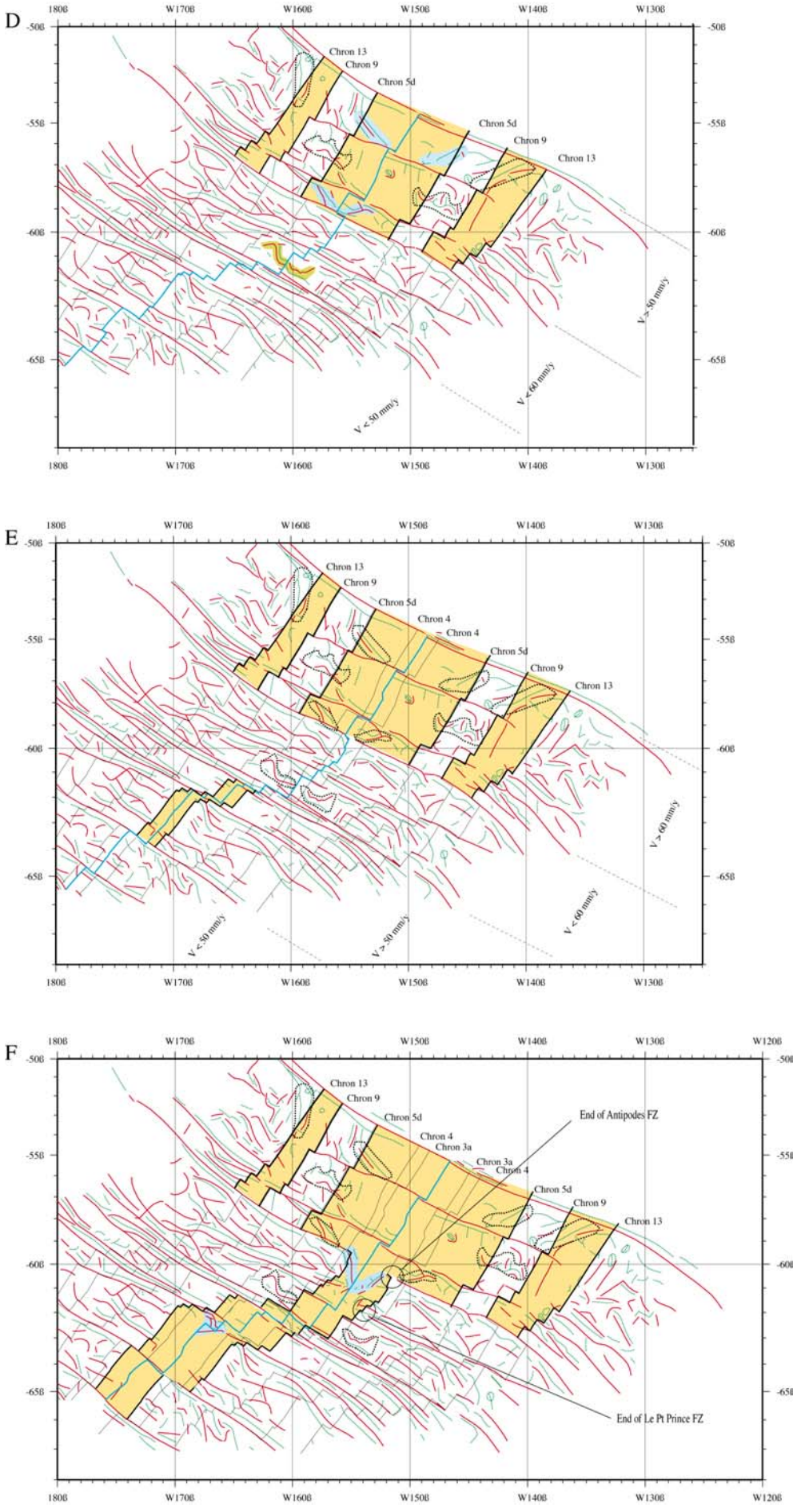

Plate 8 Continue

6. Effects of Spreading Rate on Axial Morphology and Seafloor Roughness

The spreading rate is clearly the first-order, key parameter that governs the observed transition in axial morphology (from an axial valley in the southwestern end to an axial high in the northeastern and of our study area) and the observed changes in seafloor roughness since 35 Ma. However, changes in seafloor roughness do not follow exactly the same spreading rate dependence as changes in axial morphology [*Small and Sandwell*, 1992; *Small*, 1994]. For instance, an axial valley is present south of Pitman FZ and in some places in the transitional area, while seafloor is smooth for crustal ages younger than 5 to 6 Ma. This suggests that abyssal hills generated at axial highs always result in smooth seafloor. In contrast, smooth seafloor does not mean necessary present-day axial high. This observation, based on our qualitative analysis of seafloor roughness, is consistent with previous, quantitative studies showing that abyssal hills generated at axial high mid-ocean ridges display little if any functionality with spreading rate, in contrast with those generated at axial valleys [*Goff*, 1991; *Macario et al.*, 1994].

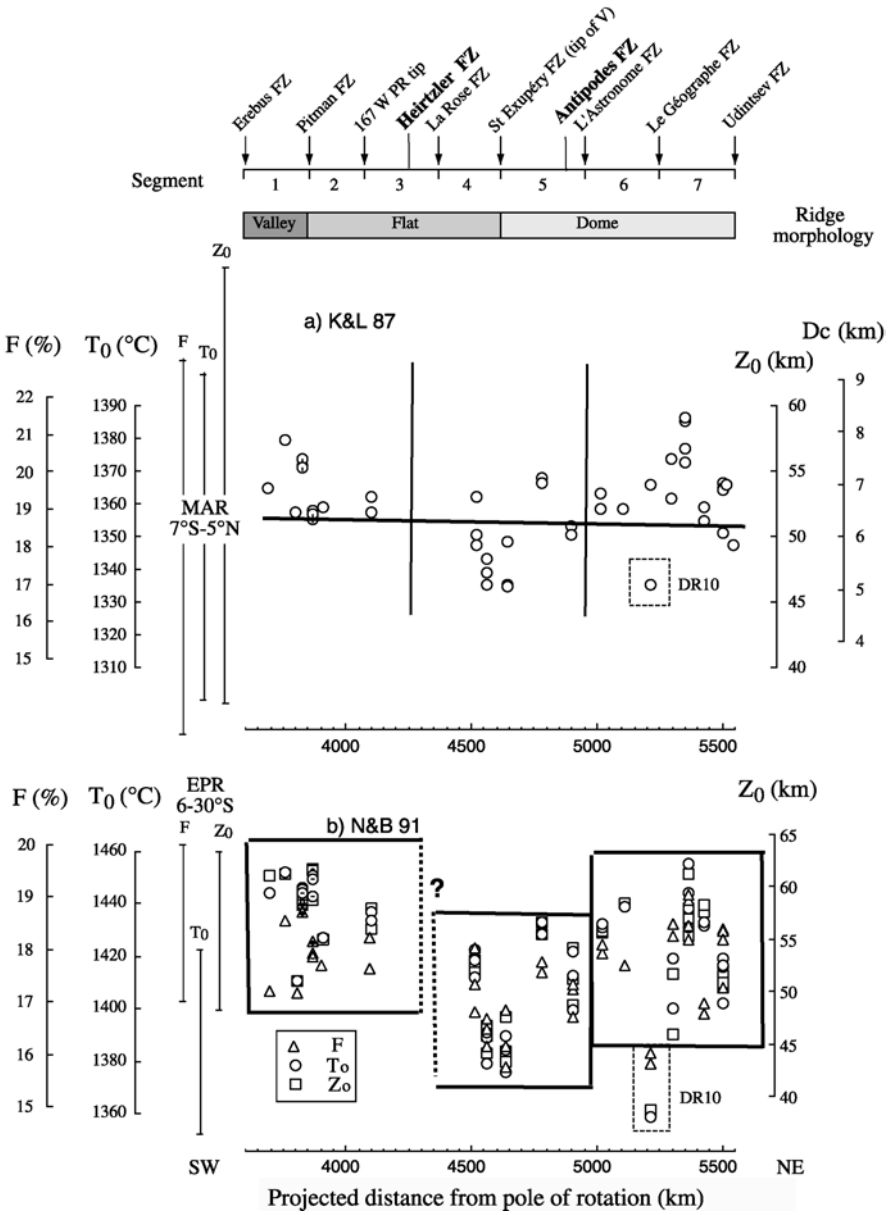

Figure 11. PAR thermal structure inferred from major element melting models calculations (K&L 87, *Klein and Langmuir* [1987] model; N&B 91, *Niu and Batiza* [1991] model, reproduced after Figure 6 of *Vlastelic et al.* [2000] (see their paper for explanations and for the complete figure caption). The difference with Vlastelic et al. Figure 6 lies in the interpretation of the geographical distribution of the geochemical variation. *Vlastelic et al.* [2000] focus on the lack of correlation between geochemistry and present-day axial morphology. Here, we identify three different geochemical domains (each box represents one domain) and argue that a correspondance exists between geochemical variations and seafloor roughness variations: Independent results from geochemical models and from seafloor roughness analysis indicate that the upper mantle temperature is likely to be cooler somewhere between Antipodes and La Rose FZ. The question mark indicates that the domain boundaries that we propose are not very well defined owing to poor geochemical sampling.

The different models for explaining the spreading rate dependence of axial introduce the concept of a threshold spreading rate that is mantle temperature dependent. Increases in mantle temperature do produce rheological changes (by decreasing the viscosity of the upper mantle and the thickness and strength of the crust) that allow the morphological transition from axial valley to axial high to occur at slower spreading rates mantle [*Neumann and Forsyth*, 1993; *Chen and Morgan*, 1990a, 1990b]. Consequently, the threshold spreading rate value is expected to increase when the upper mantle temperature decreases. Using major element data sets (from 20 dredges collected between 65°S and 56°S) and two different petrological melting models [*Klein and Langmuir*, 1987; *Niu and Batiza*, 1991], *Vlastelic et al.* [2000] have attempted to infer the pattern of upper mantle temperature variations beneath the Pacific-Antarctic south of Udintsev FZ (Figure 11) and focused on the lack of correlation between geochemistry and present-day axial morphology. However, at the segment scale, changes in axial morphology are not recorded by the geochemical properties of the ridge basalts (except the cooling effects of fracture zones), and at wavelengths of ~ 700 km, three sections appear: below the central section, the upper mantle temperature is inferred to be 30° to 40°C cooler than below the two adjacent sections. In the cool area (approximately centered on Saint Exupéry FZ), the transition from rough to smooth seafloor occurs for spreading rates >60-65 mm/yr, while the threshold value is anywhere else equal to 50 mm/yr. As expected, the cooler the mantle temperature, the higher the threshold value of the rough/smooth transition. Both geochemical and seafloor roughness data consistently suggest that the upper mantle is segmented with a wavelength of about ~700 km.

7. Conclusion

The Pacific-Antarctic Ridge between 180°W and Udinsev FZ is characterized by a 650-km-long transitional section where the axial morphology alternates between axial valley, axial high, or flat profiles. In this transitional section the mechanical properties of the axial lithosphere are close to the threshold between slow spreading and fast spreading ridges. Owing to the proximity of the Euler pole of rotation between the Pacific and Antarctic Plates, the geometry of the plate boundary evolves rapidly in response to Pliocene changes in the Pacific/Antarctic relative motion. Clearly, different types of adjustment occur, either by the initiation of propagating rifts or by transitions from transform faults into giant overlapping spreading centers.

What we observe in the present-day transitional area is representative of the phenomena that have occurred since 35 Ma:

Increases in spreading rate above the threshold value produced rheological changes that resulted in transitions from rough to smooth seafloor topography. Owing to a general increase in the angular rotation rate between Pacific and Antarctic, the transitional area has progressively migrated southward since 35 Ma, creating the V shaped of the rough to smooth boundary east of 157°W.

Clockwise rotations of the spreading direction were accommodated by the plate boundary; in the transitional area (past and present), these rotations resulted either in rift propagation, either in transitions from fracture zones to non transform discontinuities that left the trails on the seafloor that presently delineate the 1000 km large V shaped boundary. The V shape appears to be most entirely related to changes in the relative plates motion.

In addition, the detailed study of the evolution of seafloor roughness variations since 35 Ma reveals the existence of a 700-km wavelength segmentation of the PAR south of Udintsev FZ, with a relatively cool area approximately centered on Saint Exupéry FZ. It is worthwhile to note that this segmentation is consistent with the long-wavelength segmentation of the East Pacific Rise inferred from the filtered Pacific geoid [*Cazenave et al.,* 1992]. Further studies are needed to investigate the relationship between this 700-km-long segmentation and the temperature pattern of the Pacific upper mantle.

Acknowledgments. We thank the captain and crew of the R/V *L'Atalante* for making this study possible. Dave Sandwell kindly provided the 1-min gravity grid of the Pacific-Antarctic area before publication and Steve Cande gave helpful advice. All the figures have been drawn using GMT freeware [*Wessel and Smith*, 1995].

References

Aslanian, D., H. Ondréas, L. Géli, and A. Briais, Axial morphology of the Pacific-Antarctic Ridge from the PACANTARCTIC cruise of the N/O L'Atalante (abstract), *Eos Trans. AGU, 77*(46), Fall Meet. Suppl., 729, 1996.

Augustin, J. M., C. Edy, B. Savoye, and E. Le Drezen, Sonar mosaic computation from multibeam echo sounder, *Proceedings in IEEE Oceans 94 - Brest,* vol. II, pp. 433-438, Piscatawary, N.J., 1994.

Bourillet, J. F., C. Edy, F. Rambert, C. Satra, and B. Loubrieu, Swath mapping system processing: Bathymetry and cartography, *Mar. Geophys. Res., 18*, 487-506, 1996.

Briais, A., Structural analysis of the segmentation of the Central Indian Ridge between 20°30'S and 25°30'S (Rodriguez Triple Junction), *Mar. Geophys. Res.*, *17*, 431-467, 1995.

Briais, A., D. Aslanian, H. Ondréas, and L. Géli, The 167°W propagator along the Pacific-Antarctic Ridge: Results from the Pacantarctic cruise (abstract), *Eos Trans. AGU,* 77(46), Fall Meet. Suppl., 729, 1996.

Cande, S.C., and D.V. Kent, Revised calibration of the geomagnetic polarity timescale for the Late Cretaceous and Cenozoic, *J. Geophys. Res*., *100*, 6093-6095, 1995.

Cande, S.C., C.A. Raymond, J. Stock, and W. F. Haxby, Geophysics of the Pitman Fracture Zone and Pacific-Antarctic Plate motions during the Cenozoic, *Science, 270*, 947-953, 1995.

Cazenave, A., S. Houry, B. Lago, and K. Dominh, Geosat-derived geoid anomalies at medium wavelength, *J. Geophys. Res*., *97*, 7081-7096, 1992.

Chen, Y., and J.W. Morgan, Rift valley/no rift valley transition at mid-ocean ridges, *J. Geophys. Res*., *95*, 17,571-17,581, 1990a.

Chen, Y., and J.W. Morgan, A nonlinear rheology model for mid-ocean ridge axis topography, *J. Geophys. Res., 95*, 17,583-17,604, 1990b.

Cochran, J. R., J. C. Sempéré, and SEIR Scientific Team, The Southeast Indian Ridge between 88°E and 118°E: Gravity anomalies and crustal accretion at intermediate spreading rates, *J. Geophys. Res., 102*, 15,463-15,487, 1997.

Géli, L., et al., Evolution of the Pacific-Antarctic Ridge South of the Udintsev Fracture Zone, *Science,* 278, 1281-1284, 1997.

Géli, L., D. Aslanian, J. L. Olivet, I. Vlastelic, L. Dosso, H. Guillou, and H. Bougault, Location of Louisville hotspot and origin of Hollister ridge: Geophysical constraints, *Earth Planet. Sci. Lett., 164*, 31-40, 1998.

Goff, J. A., A global and regional stochastic analysis of near-ridge abyssal hill morphology, *J. Geophys. Res., 96*, 21,713-21,737, 1991.

Hey, R. N., M. C. Kleinrock, S. P. Miller, T. M. Atwater, and R. C. Searle, Sea Beam/Deep Tow investigation of an active oceanic propagating rift system, Galapagos, 95,5°W, *J. Geophys. Res., 91*, 3369-3393, 1986.

Klein, E. M., and C. H. Langmuir, Global correlations of oceanic ridge basalt chemistry with axial depth and crustal thickness, *J. Geophys. Res*., *92*, 8089-8115, 1987.

Lonsdale, P., Structural geomorphology of the Eltanin Fault System and adjacent transform faults of the Pacific-Antarctic plate boundary, *Mar. Geophys. Res., 16*, 105-143, 1994a.

Lonsdale, P., Geomorphology and structural segmentation of the crest of the southern (Pacific-Antarctic) East Pacific Rise, *J. Geophys. Res., 99*, 4683-4702, 1994b.

Macario, A., W. F. Haxby, J. A. Goff, W. B. F. Ryan, S. C. Cande, and C. A. Raymond, Flow line variations in abyssal hill morphology for the Pacific-Antarctic Ridge at 65°S, *J. Geophys. Res.*, *99*, 17,921-17,934, 1994.

Macdonald, K. C., Tectonic and magmatic processes on the East Pacific Rise, in *The Geology of North America*, vol. N, The Eastern Pacific Ocean and Hawaii, pp. 93-110, Boulder, Colo., Geol. Soc. of Am., 1989.

Macdonald, K. C., J. C. Sempéré, and P. J. Fox, Reply to comment on "The debate concerning overlapping spreading centers and mid-ocean ridge processes," *J. Geophys. Res., 91*, 10,501-10,510, 1986.

Macdonald, K. C., D. Scheirer, and S. M. Carbotte, Mid-Ocean Ridges: Discontinuities, segments and giant cracks, *Science, 253*, 986-994, 1991.

Macdonald, K. C., et al., The East Pacific Rise and its flanks 8-18°N: History of segmentation, propagation and spreading direction based on Sea Beam studies, *Mar. Geophys. Res., 14*, 299-344, 1992.

Neumann, G. A., and D. W. Forsyth, Comparison of marine gravity from shipboard and high-density satellite altimetry along the Mid-Atlantic Ridge, 30.5°-35.5°S, *Geophys. Res. Lett., 20*, 1639-1642, 1993.

Niu, Y., and R. Batiza, An empirical method for calculating melt compositions produced beneath mid-ocean ridges: Application for axis and off-axis (seamounts) melting, *J. Geophys. Res., 96*, 21,753-21,777, 1991.

Sahabi, M., L. Géli, J. L. Olivet, L. Gilg-Capar, G. Roult, H. Ondréas, P. Beuzart, and D. Aslanian, Morphological reorganization within the Pacific-Antarctic Discordance, *Earth Planet. Sci. Lett., 137*, 157-173, 1996.

Sempéré, J. C., J. R. Cochran, and the SEIR Scientific Team, The Southeast Indian Ridge between 88°E and 118°E: Variations in crustal accretion at constant spreading rate, *J. Geophys. Res., 102*, 15,489-15, 506, 1997.

Small, C., A global analysis of mid-ocean ridge axis topography, *Geophys. J. Int*., *116*, 64-84, 1994.

Small, C., and D. T., Sandwell, An analysis of ridge axis gravity roughness and spreading rate, *J. Geophys. Res.*, *97*, 3235-3245, 1992.

Smith, W.H, and D.T. Sandwell, Marine gravity field from declassified Geosat and ERS-1 altimetry (abstract), *Eos Trans AGU*, *76*(46), Fall Meet. Suppl., 156, 1995.

Tebbens, S.F., and S.C. Cande, Southeast Pacific tectonic evolution from early Oligocene to Present, *J. Geophys. Res., 102*, 12,061-12,084, 1997.

Vlastelic, I., L. Dosso, H. Guillou, H. Bougault, L. Géli, J. Etoubleau, and J. L. Joron, Geochemistry of the Hollister ridge: Relation with the Louisville hotspot and the Pacific-Antarctic Ridge, *Earth Planet. Sci. Lett., 160*, 777-793, 1998.

Vlastelic, I., L. Dosso, H. Bougault, D. Aslanian, L. Géli, J. Etoubleau, M. Bohn, J. L. Joron, and C. Bollinger, Chemical systematics of an intermediate spreading ridge: The Pacific-Antarctic Ridge between 56 and 66°S, *J. Geophys. Res., 105*, 2915-2936, 2000.

Wessel, P., and W. H. F. Smith, New version of the Generic Mapping Tools released, *Eos Trans. AGU*, *76*(46), 329, 1995.